Original

Ocana, V.; Zorita, E.; Heimbach, P.:

Stochastic secular trends in sea level rise

Journal of Geophysical Research : Oceans (2016) AGU

DOI: 10.1002/2015JC011301

AGU PUBLICATIONS

JGR

Journal of Geophysical Research: Oceans

RESEARCH ARTICLE

10.1002/2015JC011301

Stochastic secular trends in sea level rise

Victor Ocaña[1], Eduardo Zorita[2], and Patrick Heimbach[3,4]

[1]Department of Earth, Atmospheric and Planetary Sciences, Massachusetts Institute of Technology, Massachusetts, USA, [2]Institut für Küstenforschung, Helmholz-Zentrum Geesthacht, Geesthacht, Germany, [3]Institute for Computational Engineering and Sciences, The University of Texas at Austin, Austin, Texas, USA, [4]Institute for Geophysics, The University of Texas at Austin, Austin, Texas, USA

Key Points:
- The hypothesis of a stochastic centennial trend in observed GMSL cannot be rejected and is physically sound
- GMSL variability is partly generated by integrated red noise, possibly causing natural multicentennial trends
- Reconstruction and measurements errors in GMSL can cause spurious multidecadal or longer trends comparable to physical ones

Correspondence to:
V. Ocaña,
vocana@mit.edu

Citation:
Ocaña, V., E. Zorita, and P. Heimbach (2016), Stochastic secular trends in sea level rise, *J. Geophys. Res. Oceans*, *121*, 2183–2202, doi:10.1002/2015JC011301.

Received 6 OCT 2015
Accepted 2 MAR 2016
Accepted article online 7 MAR 2016
Published online 2 APR 2016

Abstract Global mean sea level (GMSL) has been rising since (at least) the nineteenth century and the rate of rise may be increasing. Several studies that attempt to explain the long-term trend of GMSL during the instrumental record share the common assumption that this trend is deterministic in nature and different from natural variations. Here we show that the trend can alternatively be explained, at least in part, as being caused by random variations within the coupled ocean-atmosphere-cryosphere system, and hence not having a deterministic origin. These random trends, which add to externally forced changes (e.g., through anthropogenic climate change), are a consequence of the integrated character of GMSL, which is the cumulative addition of temporal contributions that exhibit random character, and whose integration results in GMSL variations with persistence on decadal-centennial time scales. The generation of trends by integration of random stationary noise (i.e., even in a constant climate) is a robust and fundamental feature of stochastically forced systems with memory. The integrated character of GMSL results in an intrinsic difficulty in distinguishing internal from externally forced trends.

1. Introduction

Sea level and its evolution in time are of great interest for at least two reasons: the potential impact on coastal populations and ecosystems is large [e.g., *Nicholls et al*., 2007, and the references therein] and the imprint of the physical climate system on sea level may make it an indicator of climate change (see the Intergovernmental Panel on Climate Change Fifth Assessment Report, in the following IPCC-AR5) [*Stocker et al*., 2013]. In this study, we investigate the degree to which GMSL rise may be explained by random natural variations in addition to deterministic processes.

GMSL exhibits variability on time scales of months to millennia. On a centennial time scale, which is the main focus of this study, there is broad consensus that GMSL has increased by ∼0.2 m since the nineteenth century, with interannual to interdecadal variations around the long-term trend [e.g., *Hay et al*., 2015; *Church and White*, 2006, 2011; *Jevrejeva et al*., 2008, chapters 3 and 13 of the IPCC-AR5]. It has been proposed that GMSL has been nearly constant over the last 2–3 kyr BP [e.g., *Lambeck et al*., 2004, 2010; *Nicholls and Cazenave*, 2010], even though there is extensive evidence of multidecadal to centennial GMSL variability from proxi-based reconstructions [e.g., *Cronin*, 2011, 2012; *Schaefer et al*., 2009; *Kemp et al*., 2011; *Marzeion et al*., 2014], AOGCM simulations [e.g., *Gonzalez-Rouco et al*., 2006; *Gregory et al*., 2006], and semiempirical models [e.g., *Grinsted et al*., 2010; *Vermeer and Rahmstorf*, 2009]. Averaged over the last 2 kyr, IPCC-AR5 estimates that the rate of sea level rise has been in the range of a few tenths of a mm/yr and gives an upper limit to changes in sea level of ±0.25 m on time scales of a few hundred years (cf. ∼0.20 m in a time period of 150–200 years from the instrumental record). GMSL changes of similar and larger magnitude might not have been unusual in the past [*Rohling et al*., 2008; *Grant et al*., 2012; *Kopp et al*., 2013, chapter 5 of IPCC-AR5], with average rates of sea level rise of 0.4–1.6 m per century (around 2–10 times larger than present rates of change) during the last interglacial around 120 kyr before present (this period is often used as an analog for present-day climatic conditions) [*Otto-Bliesner et al*., 2013]. The question naturally arises whether the observed GMSL rise in the instrumental record can be distinguished from variations that are not induced by external deterministic forcing factors (e.g., anthropogenic climate change or millennial changes in solar energy reaching the earth's surface), but rather are a consequence of the integration by the ocean-cryosphere system of random changes in energy and fresh water fluxes in the ocean.

Fluctuations of GMSL are driven by changes in the energy flux through the ocean surface and fresh water flux from land ice masses. In this study, we consider random fluctuations of these fluxes that have zero mean and are stationary but may have persistence in time, causing periods of nonzero sample mean and local trends. We define natural variability of GMSL as caused by the integration of these random fluctuations. This definition of "natural" variability is *not* equivalent to the standard definition of "internal" variability (understood as caused by the exchanges among atmosphere, ocean, and cryosphere seen as a closed system with no changes in fluxes external to them) of the atmosphere-ocean system, since it includes forcings that are external to the ocean but not deterministic in nature, like the energy imbalances caused by volcanic eruptions.

At each time t, GMSL anomaly, h, with respect to a given reference level, is the integral of the past contributions up to that moment

$$h(t)=\int_{t_0}^{t}(\dot{h}_T+\dot{h}_E)dt=\int_{t_0}^{t}(f(F)+g(M))dt \tag{1}$$

where h_T is the thermosteric sea level change, due to the expansion of the water column following exchanges of heat between the ocean and the atmosphere (F). h_E is the barystatic sea level change [*Gregory et al*., 2013], due to the changes in the mass balance of glaciers/ice caps, Antarctica and Greenland (M). Other contributions such as the heat exchange with the lithosphere, changes in volume associated with haline contraction, terrestrial water storage, and net imbalances in precipitation minus evaporation over the oceans, are of smaller magnitude [e.g., *Antonov et al*., 2002; *Church and White*, 2011; *Munk*, 2002] and can be neglected as a first approximation. The origin t_0 is an arbitrary time origin that sets the GMSL reference level.

The form of the functions $f(F)$ and $g(M)$ can be determined from basic physical principles (see Appendix A), and equation (1) can be readily discretized to yield

$$h(t+\Delta t)=h(t)+\lambda F(t)\Delta t+\beta M(t)\Delta t \tag{2}$$

where to zeroth order approximation, the heat and fresh water fluxes into the ocean are independent of current sea level $h(t)$. Parameters λ and β are respectively the "expansion efficiency of heat" [*Russell et al*., 2000] and a simple conversion factor from units of mass of water to equivalent volume height (in mm). We follow the approximation that $F(t)$ and $M(t)$ are independent physical processes, even though they may be correlated if they are driven by the same random forcing. Both the linear approximation for $f(F)$ and $g(M)$ and their independence follow from the approximation of constant density and heat capacity of sea water, and the fact that the addition of fresh water and energy from land ice melting is small compared to the volume of the ocean.

Equation (2) has the form of a stochastic process in which the ocean integrates random variations (and other external forcings, possibly deterministic, that may be present in F and M), creating variability that is not only due to an external deterministic forcing. The theoretical foundations of stochastic climate processes have been studied [e.g., *Hasselmann*, 1976] and the existence of climate and oceanic phenomena that can be characterized as integrated processes has long been recognized [e.g., *Frankignoul and Hasselmann*, 1977; *Wunsch et al*., 2007; *Fraedrich et al*., 2009]. Equation (2) includes no feedback, leading to a nonstationary process with unbounded variance, and its validity is restricted to a temporal range $\tau_m < t < \tau_M$, defined by time scales (τ_m, τ_M) typical of the physical process under consideration (a "two-timing" theory) [see *Hasselmann*, 1976].

If F and M have a nonzero mean or even include a deterministic trend, this would induce a trend in GMSL not related to natural variability. In the absence of a deterministic external forcing, one would expect the heat exchange between atmosphere and ocean, and the mass balance of ice sheets and glaciers, to be a stationary processes with zero mean, but both F and M may exhibit persistence in time not related to an external forcing or oscillatory processes, and can be characterized as red noise with periods of trend-like behavior and nonzero sample mean [e.g., *Box and Colgan*, 2013; *Leclercq et al*., 2011; *Frezzotti et al*., 2013; *Andersen et al*., 2006]. As we shall see (section 3), these periods may extend for several decades and it may be difficult to identify them as either multidecadal variability or externally forced trends, in time series that extend for only about a century. Notice that the stochastic model proposed by *Hasselmann* [1976]

introduces the basic concept that even uncorrelated atmospheric white noise, when integrated by the ocean, can generate low frequency variability in the latter. We face here a more complex situation, in that the random forcing integrated by the ocean in equation (2) may be itself red noise, consequently generating variability at even lower frequencies.

Several studies have tried to estimate the fraction of the observed GMSL trend that can be attributed to natural variations [e.g., *Dangendorf et al*., 2014; *Becker et al*., 2014; *Jorda*, 2014; *Church and White*, 2011; *Jevrejeva et al*., 2008], all sharing the common a priori assumption that the long-term trend spanning the period covered by the instrumental record is not a stochastic trend. In contrast, we set out to study this assumption, by testing the null hypothesis that such a long-term trend can be stochastic in nature and can be caused by random forcings. For the thermosteric component of GMSL, e.g., *Marcos and Amores* [2014], *Gleckler et al*. [2012], *Slangen et al*. [2014], and *Church et al*. [2013a] compare observed time series with the ensemble mean of several model simulations, even though "[c]limate models [. . .] display a large spread of outputs with limited correspondence with the observationally based estimates of thermosteric sea level" [*Marcos and Amores*, 2014]. The contribution of fresh water from glaciers to GMSL has often been studied with dynamical models that include the possibility of natural variability caused by random forcings [e.g., *Marzeion et al*., 2012, 2014; *Church et al*., 2013a; *Roe and O'Neal*, 2009; *Roe*, 2011] concluding that natural variability can cause glacier length and mass changes on centennial time scales similar to the estimated changes in the past millennium (e.g., *Marzeion et al*. [2014] estimate that "only $25 \pm 35\%$ of the global glacier mass loss during the period from 1851 to 2010 is attributable to anthropogenic causes").

Some of these studies propose trend stationary models that fit a deterministic trend and base their main conclusions, like magnitude and significance of linear and higher-order trends, on standard techniques like least squares estimates [e.g., *Church and White*, 2006, 2011; *Jevrejeva et al*., 2008; *Marcos and Amores*, 2014]. Different choices of models, data and specific techniques, lead to different estimates of GMSL and its trends [e.g., compare *Hay et al*., 2015; *Church and White*, 2011; *Jevrejeva et al*., 2008; *Wenzel and Schröter*, 2010; *Ray and Douglas*, 2011; *Holgate*, 2007; *Houston and Dean*, 2011] and prompts for the study of alternative explanations of the GMSL long-term trends. There is ample literature discussing the relative advantages and shortcomings of these statistical methods and the special difficulties that MSL time series and reconstructions present, like subsampling, temporal and spatial averaging, finite size of the time series compared to the time scales studied, model choice (e.g., linear trend versus higher order), underlying assumptions for residuals and their effect on statistical inference, etc. [see e.g., *Foster and Brown*, 2015; *Christiansen et al*., 2010; *Visser et al*., 2015; *Hay et al*., 2015; *Solow*, 1990; *Cronin*, 2011; *Wu et al*., 2007; *Schmith et al*., 2012]. To address some of these issues, others have proposed "long memory" processes and fractionally differenced (FD) models [e.g., *Dangendorf et al*., 2014; *Becker et al*., 2014]. Long memory is by definition an asymptotic property, notably difficult to identify in finite time series and to distinguish from other representations, for instance autoregressive-moving average models [see e.g., *Foster and Brown*, 2015; *Palma*, 2007; *Percival et al*., 2001], and we consider important to test whether these simpler models can appropriately describe the fluxes F and M, and GMSL.

This paper investigates whether the null hypothesis "GMSL increase in the instrumental record is due to natural variability" can be rejected, and whether the long-term trend can *only* be explained by deterministic external forcing factors. One common source of confusion should be clarified from the onset: the failure to reject the null hypothesis of the long-term trend being stochastic does *not* imply accepting it. This paper presents an alternative to the purely deterministic trend model and does not claim the stochastic trend model to be the correct or only explanation for the observed GMSL trend. We pursue two separate, yet convergent, lines of evidence. In section 3, we characterize F and M as random processes and derive their statistical properties. In particular, we show that the null hypothesis that both F and M are stationary and have zero mean, cannot be rejected. Furthermore, we explore whether present estimates of h_T and h_E are consistent with an integrated process forced with stationary (red) noise. Section 4 shows that the longest available GMSL reconstructions can be characterized as integrated processes. In section 5, we illustrate the results of the previous sections with synthetic time series that simulate the processes modeled. Section 6 concludes.

2. Data and Methods

2.1. Data

The time series used in this study are summarized in Table 2. Units are converted where necessary to W/m^2, mm, and mm/yr for heat flux, GMSL, and GMSL rate of change, respectively. All time series are globally

Table 1. List of Symbols and Acronyms[a]

h	Globally averaged mean sea level (GMSL)
h_T	Thermosteric component of GMSL
h_E	Barystatic component of GMSL
F	Air-sea heat flux
N	Radiation imbalance at the top of the atmosphere
Q	Heat content of the ocean
M	Fresh water flux into the ocean
λ	Expansion efficiency of heat
β	Units conversion factor from mass of water to equivalent volume height
A	Snow accumulation
R	Melt water runoff
L_M	Marine ice loss
Δ	Difference operator
B	Backshift operator
$\phi(B)$	Autoregressive polynomial of an ARIMA process
$\theta(B)$	Moving average polynomial of an ARIMA process
a	Drift in an ARIMA process
d, d_e	Order of integration and its GPH estimate
ω	Frequency
$\Phi(\omega)$	Spectral density
μ	Mean (or sample mean) of a stochastic process
σ^2	Variance (or sample variance) of a stochastic process
ρ	Lag-1 autocorrelation (or sample autocorrelation) coefficient
τ	Linear trend of a time series
ϵ	Random noise component in an ARIMA process
ζ	Measurement or reconstruction error
GMSL	Global mean sea level
ARIMA(p, d, q)	Autoregressive-Integrated-Moving average process
AR(p)	Autoregressive process of order p
MA(q)	Moving average process of order q
SDF	Spectral density function
MB	Total mass balance of an ice sheet
SMB	Surface mass balance
C11, CM	GMSL reconstruction by *Church and White* [2011]
JE, JM	GMSL Reconstruction by *Jevrejeva et al.* [2008]

[a]In the text, quantities with hat "^" denote actual values without errors; quantities with tilde "~" refer to the reconstruction errors.

averaged quantities. *Hanna et al.* [2011] provide only time series for surface mass balance and runoff, and we combine these to produce a time series of net mass balance using the hybrid linear-quadratic parametrization used by *Box and Colgan* [2013]. There are several estimates of the quantities studied in this work, and we chose, whenever available, at least two for each of them, that are described in peer-reviewed literature, and either differ substantially from one another or are obtained by different methods or models.

To conduct our analysis of GMSL, $h(t)$, we focus on the reconstructions by *Church and White* [2011] (C11) that runs from 1880 to 2009 and *Jevrejeva et al.* [2008] (JE) from 1700 to 2002 (Figure 3). C11 was made available to us with monthly resolution (denoted CM) and performed without filtering the Permanent Service for Mean Sea Level (PSMSL) data. JE is available only with annual resolution, but an earlier version [*Jevrejeva et al.*, 2006] denoted JM, which is virtually identical to JM after 1850, is available also with monthly resolution. The reconstructions are not homogeneous in time, with reconstruction errors and year-to-year variations changing markedly

Table 2. Data Sets Used in This Study[a,b]

Reference	Quantity	Units	Time Period	Resolution	Notes
Wunsch and Heimbach [2013a]	F	W/m^2	1993–2011	Month	Data assimilation in a OGCM
Allan et al. [2014]	N	W/m^2	1985–2013	Month	
Levitus et al. [2012]	Q	10^{22} J	1955–2011	3 month	
Ishii and Kimoto [2009]	Q	10^{22} J	1950–2013	Year	Corrects temperature versus depth measurement bias
Levitus et al. [2012]	h_T	mm	1955–2011	3 month	
Gonzalez-Rouco et al. [2006]	h_T	mm	1000–1990	Year	AOGCM simulation, 900 years Natural and anthropogenic forcing
Gregory et al. [2006]	h_T	mm	1500–2000	Year	AOGCM simulation, 500 years Only natural forcing
Leclercq et al. [2011]	h_E	cm SLE	1800–2005	Year	21 year running average smoothed
Marzeion et al. [2012]	M_{IC}	mm/yr SLE	1900–2011	Year	Modeled glacier contribution
Box and Colgan [2013]	M_G	mm/yr SLE	1840–2011	Year	Greenland MB
Hanna et al. [2011]	*SMB*	km^3/yr WE	1860–2010	Year	Greenland SMB
Frezzotti et al. [2013]	*SMB*		1200–2000	Year	Normalized anomalies, unitless
Church and White [2011]	h	mm	1880–2010	Month	Optimal interpolation method
Jevrejeva et al. [2008]	h	mm	1700–2002	Year	Virtual station method Available in monthly resolution 1880–2002

[a]Resolution indicates the finest time resolution available; spatially, all time series are globally averaged quantities.
[b]The symbols and acronyms in column "quantity" are explained in Table 1.

through the reconstruction period. For this reason, we analyze separately C11/CM in the time period 1930–2010 and JE/JM in the period 1885–2002 (these are the points farthest back in the past from which the time series seem to be homogeneous).

2.2. Reconstruction Errors

All time series used in this study contain "reconstruction errors", that are a consequence of measurement errors, parameterizations in models, and data processing (we refer the reader to the original references in Table 2), which, being possibly of magnitude similar to the natural variations of GMSL, play a crucial role in the description of the time series and the processes generating them. One source of errors in GMSL reconstructions is spatial subsampling [e.g., *Wunsch*, 2016; *Ray and Douglas*, 2011; *Merrifield et al.*, 2009; *Hamlington and Thompson*, 2015] combined with the fact that SL has local and regional trends that vary geographically [e.g., *Church et al.*, 2013b; *Milne et al.*, 2009]. *Hamlington and Thompson* [2015] show that for different sets of tide gauge stations used in recent studies for GMSL reconstructions, 20 year trends differ by 1–3 mm/yr throughout the twentieth century. Similarly, the satellite altimetry derived trend in GMSL rise from the AVISO database (http://www.aviso.oceanobs.com/) in the period 1993–2013 is 2.87 mm/yr while the trend in the Northern Hemisphere (NH) in the same period is 2.20 mm/yr, implying that estimating GMSL with the NH (even if it was known with no error), as is typical of the first decades of the reconstructions, would introduce a spurious trend of 0.67 mm/yr on a time scale of 20 years.

A second cause of time-structure in GMSL reconstruction errors is that formally first differences of GMSL, $\Delta h(t)$, are reconstructed, to avoid the problem of absence of a common datum between PSMSL records [e.g., *Ray and Douglas*, 2011; *Hay et al.*, 2015; *Church and White*, 2006]. Differencing is performed on the time series of the individual tide gauge station data, which, assuming a white noise additive measurement error, introduces a moving average (MA) structure in the error of the differenced series [e.g., *Box et al.*, 2008]. GMSL differences are then reconstructed from the individual differenced series, and new errors are introduced in the process [e.g., *Church and White*, 2006; *Jevrejeva et al.*, 2006]. Even if the latter are white noise, the error in $\Delta h(t)$ will have at least a MA structure, which when integrated to obtain $h(t)$ may introduce spurious trends in the reconstructions (even uncorrelated errors in $\Delta h(t)$ will have a power law contribution to the power spectrum of $h(t)$) [*Ray and Douglas*, 2011; *Foster and Brown*, 2015]. The reconstruction error in $h(t)$ "propagates" in the direction of integration (e.g., backward in time in *Church and White* [2011]) and the RMS of the difference between the actual and reconstructed values of $h(t)$ increases in that direction. A reconstruction error in $\Delta h(t)$ with std 2.5 mm (monthly resolution, with no autocorrelation and uncorrelated to $\Delta h(t)$, cf. errors of 1–5 mm in GMSL from satellite altimetry, e.g., *Tai and Wagner* [2011], *Masters et al.* [2012], *Ablain et al.* [2009], or 6–24 mm in *Church and White* [2011]) would introduce an "error trend" in the range of ± 1.61 mm/yr at the 95% confidence level, similar to the estimated linear trend of 1.60 mm/yr in the instrumental record.

2.3. Methods and Statistical Models

Several mathematical models have been used to represent stochastic processes that exhibit memory and power law spectral density functions [e.g., *Box et al.*, 2008; *Palma*, 2007; *Chandler and Scott*, 2011]. We will base our analysis on the Autoregressive-Integrated-Moving average (ARIMA) class of models, which is very general and describes a wide range of processes, given by the equations (we follow closely the notation of *Box et al.* [2008] and *Granger and Morris* [1976])

$$\begin{aligned} x(t) &= \hat{x}(t) + \zeta(t) \\ \hat{\phi}(B)\Delta^d \hat{x}(t) &= a + \hat{\theta}(B)\hat{\epsilon}(t) \\ \tilde{\phi}(B)\zeta(t) &= \tilde{\theta}(B)\tilde{\epsilon}(t) \end{aligned} \tag{3}$$

where $\hat{x}(t)$ represents the actual value of the quantity described by the time series $x(t)$, without error, and $\zeta(t)$ is the reconstruction error (throughout the text, quantities with hat "ˆ" denote actual values without errors; quantities with tilde "˜" refer to the reconstruction errors). t is time, a is a constant, $\hat{\epsilon}(t)$ and $\tilde{\epsilon}(t)$ are zero mean independent identically distributed processes and B is the backshift operator, $B[x(t)] = x(t-1)$; $\hat{\phi}(B)$ and $\hat{\theta}(B)$ (or $\tilde{\phi}(B)$, $\tilde{\theta}(B)$) are polynomials in B, of orders $\hat{p}$ and $\hat{q}$ ($\tilde{p}$, $\tilde{q}$) respectively, autoregressive (AR) coefficients $\hat{\phi}_i$ ($\tilde{\phi}_i$) and moving average (MA) coefficients $\hat{\theta}_i$ ($\tilde{\theta}_i$). $\Delta = 1 - B$ is the difference operator, and d is the order of integration.

The constant a, the *drift*, determines the mean of an ARMA processes ($d = 0$), μ, through the relation $\mu = a/(1 - \sum_{i=1}^{p} \phi_i)$. In an integrated process ($d = 1$), a introduces a linear deterministic trend $\mu \cdot t$. In the context of GMSL, a can be thought to represent an external forcing, implying that in an unforced climate state ($a = 0$), F and M will have zero (long-term) mean.

The approximation of independence between $\zeta(t)$ and $\hat{x}(t)$ implies that the variance of the reconstructed time series is simply the addition of the variances of the process without errors and the reconstruction errors

$$\sigma_{\Delta}^2 = \sigma_{\hat{\Delta}}^2 + \sigma_{\tilde{\Delta}}^2 \tag{4}$$

where subindices denote the variances of $\Delta x(t)$, $\Delta\hat{x}(t)$, and $\Delta\zeta(t)$, respectively.

Following *Box et al*. [2008] and *Granger and Morris* [1976], model (4) can be represented with a single ARIMA(p, d, q) model fitted to $x(t)$, with $p = \hat{p} + \tilde{p}$ and $q = \max[\tilde{p} + \hat{q}, \hat{p} + \tilde{q} + d]$. This model is difficult to interpret in physical terms since it lumps together the actual physical process we want to describe, $\hat{x}(t)$, and the added reconstruction and measurement errors, $\zeta(t)$, in one single variable $x(t)$. To avoid this difficulty, and be able to describe the process of interest and the additive error separately, we infer separate models for $\hat{x}(t)$ and $\zeta(t)$. Three realizations of the ARIMA model for $x(t)$ that we encounter in this study, which can be interpreted as the addition of a physical process $\hat{x}(t)$ and a reconstruction error term, are (see Appendix B and *Granger and Morris* [1976] and *Box et al*. [2008] for a complete derivation of these equivalencies and the conditions necessary for them to hold):

1. ARIMA(0, 1, 1): is an ARIMA(0, 1, 0) (a random walk) with added white noise. The corresponding model for $\Delta x(t)$ is an ARMA(0, 1).
2. ARIMA(1, 1, n): with $n = 2, 3$ is an ARIMA(1, 1, 0) with added noise and $\hat{\phi} = \phi$. The added noise in this case can be white ($n = 2$) or a MA(1) process ($n = 3$).
3. ARMA(1, 1): is an AR(1) with added white noise and $\hat{\phi} = \phi$.

The spectral density function (SDF) $\Phi(\omega)$ of an ARIMA process has a pole at zero frequency $\omega = 0$ (see for instance *Palma* [2007] and Appendix B). Under the assumption that $\zeta(t)$ and $\hat{x}(t)$ are independent of each other, and if $\zeta(t)$ can be represented by a stationary random process, the SDF of $x(t)$ at low frequencies can be approximated by the SDF of $\hat{x}(t)$ and the effect of the reconstruction errors is negligible at these frequencies. This approximation allows us to estimate d by linear regression of $log(\Phi)$ on $log(\omega)$ (the Geweke-Porter-Hudak estimator, GPH) [*Geweke and Porter-Hudak*, 1983]. In an integrated process, a noninteger value of d corresponds to a fractionally integrated process, a model frequently used to describe "long memory" [e.g., *Palma*, 2007; *Percival et al*., 2001]. Stationary processes with $d = 0$ (e.g., ARMA processes) have often a range of time scales for which Φ grows with decreasing frequency, before the SDF becomes flat at sufficiently low frequencies, but these are typically not resolved in our finite time series, and the GPH estimator will deliver a value of $d_e > 0$ even for a nonintegrated series. In this study, we use the estimated d_e of the time series only as a measure of the shape of its SDF in the frequency range available, without inferring from it the presence or absence of long memory.

3. Characterization of the Heat and Fresh Water Fluxes

3.1. Air-Sea Heat Flux and Thermosteric Sea Level Change

The net heat flux into the ocean, F, is the sum of the radiative balance (net incoming minus outgoing shortwave and longwave radiation) and turbulent heat flux (sensible and latent), that in turn explain the random character of F. IPCC-AR5 estimates that ~95% of the energy accumulated in the climate system in recent times is stored in the ocean, so we use the radiative imbalance at the top of the atmosphere N, as an independent estimate of the air-sea heat flux [*Allan et al*., 2014; IPCC-AR5, chapter 2]. Direct estimates of globally averaged F and N are thought to represent well temporal variability, but large uncertainties remain in estimates of the mean value, which is usually calibrated to match estimates from ocean heat content (OHC), Q [*Wunsch and Heimbach*, 2013a; *Large and Yeager*, 2009; *Allan et al*., 2014; *Trenberth et al*., 2014]. We compare these estimates with the heat flux inferred from OHC as $F = \frac{\Delta Q}{\Delta t}$.

Figure 1 and Table 3 summarize the main characteristics of F estimated by ECCO (Estimating the Circulation and Climate of the Oceans project) [*Wunsch and Heimbach*, 2013a], N from *Allan et al*. [2014], and F inferred

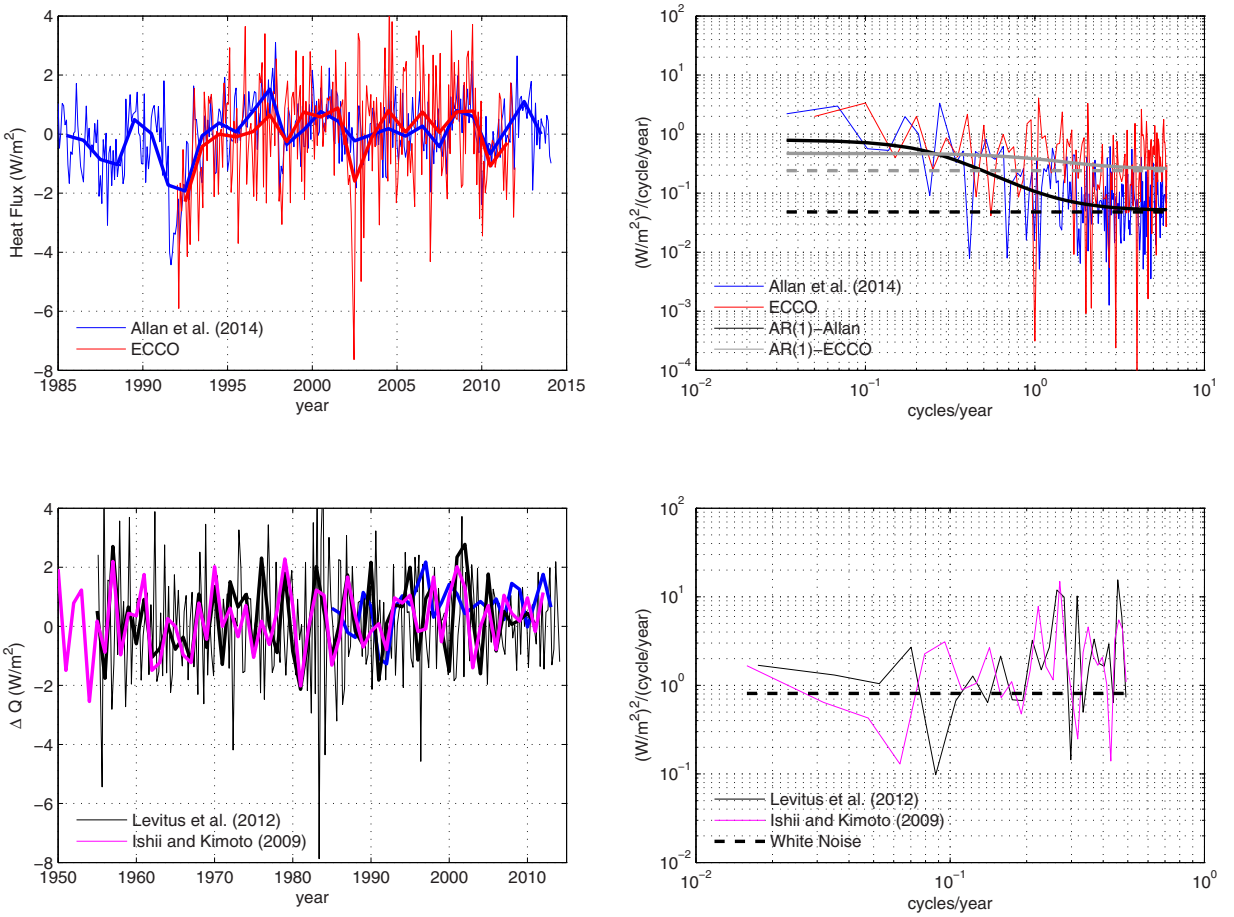

Figure 1. Heat flux into the ocean (*F*) estimated by ECCO and radiative imbalance (*N*) at the TOA from *Allan et al.* [2014] (in the top left, the mean of the respective time series has been subtracted from both series), and heat flux derived from the *Levitus et al.* [2012] and *Ishii and Kimoto* [2009] heat content estimates ((bottom left) $\frac{\Delta Q}{\Delta t}$). Thicker lines are annual means. In the bottom left, *Allan et al.* [2014] are also plotted for comparison (blue line). The right column displays the estimated periodogram (thin lines) together with the theoretical spectra of the fitted ARIMA models (thick lines).

from the OHC estimates of *Levitus et al.* [2012] and *Ishii and Kimoto* [2009]. All time series share similar characteristics, being stationary (no significant linear trend), with standard deviation of 0.75–0.86 W m^{-2}, no significant autocorrelation on time scales larger than a year and mean value statistically not different from zero. The SDF of *F* and *N* are similar, with d_e statistically not different from zero. These values are consistent with *F* being an uncorrelated zero mean stationary stochastic process, i.e., white noise, on time scales of a year or longer.

Using monthly resolution, *F* and *N* can be modeled with an ARMA(1, 1) and its associated AR(1) with added noise (Table 4), with the coefficients for *F* statistically zero. If annual averages are used the autocorrelation of *F* and *N* is zero and the simplest model is white noise. The SDF of ΔQ has the typical form of a MA(1) with negative coefficient, is flat on time scales larger than a few years and has $d_e = 0$, implying a white noise model for $\Delta\hat{Q}$, with zero mean and standard deviation derived from equation (B8) of 0.77 and 0.86 W m^{-2} for *Levitus et al.* [2012] and *Ishii and Kimoto* [2009], respectively.

The SDF of the estimated h_T in *Levitus et al.* [2012] has slope close to -2 in the log-log scale even at the lowest frequencies resolved, while Δh_T has no significant trend and positive but statistically zero mean (see Table 3). An ARIMA(0, 1, 1) (Table 4, Figure 3) produces white noise residuals, and the associated ARIMA(0, 1, 0) with added noise for $\hat{h}_T$ reproduces the spectrum of *Levitus et al.* [2012]. Further evidence for the hypothesis that $\hat{h}_T(t)$ can be represented by a random walk is found in the AOGCM simulations Erik-2 [*Gonzalez-Rouco et al.*, 2006] and nat500 [*Gregory et al.*, 2006] (Figure 3 and Tables 2 and 3). Both Erik-2 and nat500 show the characteristic SDF of an integrated process, with $d = 1$. The series of $\Delta h_T(t)$ in both simulations is consistent with white noise, notably with no negative lag-1 autocorrelation, as expected since the

Table 3. Estimated Parameters of the Air-Sea Heat Flux (F, N, ΔQ), Fresh Water Flux From Greenland and Glaciers (M_G, M_{IC}) and the Series of First Differences $\Delta h(t)$[a,b]

	Reference	μ_Δ (W m^{-2})[c]	σ_Δ (W m^{-2})	τ_Δ (W m^{-2} yr^{-1})	ρ_Δ	d_e[d]	p-MK	p-KS
F	*Wunsch and Heimbach* [2013a]	0.02 ± 0.38	0.85	−0.036 ± 0.071	0.04 ± 0.45	0.45 ± 0.76 (3)	0.11	0.59
N	*Allan et al.* [2014]	0.66 ± 0.94 [0.37][e]	0.75	−0.031 ± 0.039	0.29 ± 0.37	0.30 ± 0.58 (3)	0.23	0.49
ΔQ	*Levitus et al.* [2012]	0.22 ± 0.24	0.78 [1.25][f]	0.009 ± 0.014	−0.31 ± 0.26	−0.06 ± 0.52 (5)	0.37	0.73
ΔQ	*Ishii and Kimoto* [2009]	0.20 ± 0.23	0.86 [1.09][f]	0.009 ± 0.012	−0.19 ± 0.25	−0.06 ± 0.49 (5)	0.24	0.98
		μ (mm/Δt)[c]	σ_Δ (mm/Δt)	τ (mm/Δt^2)	ρ_Δ	d[d]	p-MK	p-KS
M_G	*Box and Colgan* [2013]	0.07 ± 0.11	0.32	3.40 ± 1.48 ($\times 10^{-3}$)	0.66	0.63 ± 0.26 (5)	0.00	0.39
M_G	*Hanna et al.* [2011]	0.04 ± 0.11	0.36	5.13 ± 1.65 ($\times 10^{-3}$)	0.52	0.51 ± 0.28 (5)	0.00	0.23
M_{IC}	*Leclercq et al.* [2011]	0.41 ± 0.34	0.36	4.04 ± 3.49 ($\times 10^{-3}$)	0.96	0.68 ± 0.54 (20)	0.00	0.01
M_{IC}	*Marzeion et al.* [2012]	1.05 ± 0.21	0.61	−4.81 ± 6.25 ($\times 10^{-3}$)	0.54	0.73 ± 0.35 (5)	0.05	0.35
	No Greenland	0.86 ± 0.10	0.39	−1.34 ± 3.26 ($\times 10^{-3}$)	0.32	0.48 ± 0.34 (5)	0.85	0.65
Δh_T	*Levitus et al.* [2012]	0.36 ± 0.55 (0.42)	1.46 [2.11][f]	0.013 ± 0.035	−0.26	1.00 ± 0.32 (2)	0.30	0.93
Δh_T	*Gonzalez-Rouco et al.* [2006]	0.02 ± 0.09	1.46	0.29 ± 0.32 ($\times 10^{-3}$)	−0.03	0.90 ± 0.13 (10)	0.20	0.00
Δh_T	*Gregory et al.* [2006]	0.02 ± 0.05	1.21	0.09 ± 0.71 ($\times 10^{-3}$)	0.24	0.98 ± 0.20 (10)	0.25	0.00
Δh	*Church and White* [2011] (**CM**)	0.18 ± 0.55 (0.35)	10.97	0.47 ± 7.80 ($\times 10^{-4}$)	−0.41	0.96 ± 0.29 (5)	0.47	0.14
	1930–2010	0.21 ± 0.54 (0.37)	8.54	1.17 ± 13.38 ($\times 10^{-4}$)	−0.36	0.93 ± 0.40 (5)	0.78	0.96
Δh	*Church and White* [2011] (**C11**)	1.65 ± 0.99 (0.74)	5.71	0.013 ± 0.020	−0.28	0.94 ± 0.30 (5)	0.28	0.97
Δh	*Jevrejeva et al.* [2006] (**JM**)	0.09 ± 0.19 (0.24)	4.75	1.06 ± 3.60 ($\times 10^{-4}$)	0.22	0.84 ± 0.24 (5)	0.04	0.00
	1885–2001	0.15 ± 0.09 (0.14)	1.75	0.86 ± 3.35 ($\times 10^{-4}$)	0.37	0.99 ± 0.38 (5)	0.32	0.67
Δh	*Jevrejeva et al.* [2008] (**JE**)	0.97 ± 2.82 (2.21)	24.90	0.009 ± 0.025	−0.24	0.91 ± 0.19 (5)	0.39	0.00
	1885–2002	1.73 ± 1.52 (1.46)	8.41	0.012 ± 0.043	−0.04	1.03 ± 0.33 (5)	0.74	0.76

[a]The value of d_e for the thermosteric and total GMSL reconstructions and simulations is that of $h_T(t)$ and $h(t)$, respectively, not of $\Delta h_T(t)$ and $\Delta h(t)$.
[b]The last two columns are p values of the Mann-Kendall (MK) test for the absence of trend and Kolmogorov-Smirnov (KS) test for normality.
[c]Sample mean confidence intervals are corrected for serial correlation.
[d]The number in parenthesis is the value of $1/\omega_{max}$, in years, used in the Geweke-Porter-Hudak estimator.
[e]Uncertainty value estimated by *Allan et al.* [2014]; in brackets, the sample mean uncertainty estimated correcting for sample size and lag-1 autocorrelation.
[f]Values estimated assuming the random walk with white error noise model described in equation (B8); values in brackets are the sample standard deviation of the time series.

simulations have no reconstruction error added. The mean of $\Delta h_T(t)$ is statistically not different from zero at 0.02 ± 0.09 and 0.02 ± 0.05 mm/yr for Erik-2 and nat500, respectively. An interesting characteristic of both simulations is that their SDF shows the form of an integrated process up to the smallest frequencies resolved, implying that the simple random walk model remains valid even on time scales of several hundred years.

3.2. Fresh Water Flux From Land Ice and Barystatic Sea Level Change

Polar ice sheets, glaciers, and ice caps are geographically disconnected and their mass balance depends on local/regional climate, i.e., temperature and precipitation, in addition to global signals like mean surface temperature [e.g., *Jacob et al*., 2012; *Cuffey and Paterson*, 2010; *Burke and Roe*, 2013; *Frezzotti et al*., 2013; *Steig et al*., 2013; *Pritchard et al*., 2012]. The barystatic component of GMSL change is characterized as the sum of three contributions

$$\frac{\Delta h_E}{\Delta t} = \beta(M_G + M_A + M_{IC}) \tag{5}$$

where M_G, M_A, and M_{IC} are solid (ice discharge) and liquid (runoff and submarine melt) freshwater fluxes from ice volume above floatation (i.e., fraction of ice masses that contributes to sea level), from Greenland, Antarctica, and glaciers/ice caps, respectively. These contributions may not be (statistically) independent of each other if they respond, at least in part, to the same forcing.

Land ice masses have complex dynamics and interactions with other components of the climate system and several mechanisms can produce variability in the fresh water fluxes from land ice masses. Surface mass balance of land ice is directly influenced by air temperature, precipitation and albedo, all of which exhibit multidecadal climate variability [see e.g., *Frezzotti et al*., 2013; *Steig et al*., 2013; *Pritchard et al*., 2012]. Furthermore, mass balance depends on the dynamics of ice flow, which have response times on a wide

Table 4. Parameters of the ARIMA(p, d, q) Models Fitted to the Reconstructions of Air-Sea Heat Flux (F, N, ΔQ), Fresh Water Flux From Greenland and Glaciers (M_G, M_{IC}), Thermosteric SL Change (h_T) and GMSL (h)[a]

	Reference	(p, d, q)	a (W m^{-2})	σ (W m^{-2})[b]	ϕ	θ	p-LBQ[c]
F	*Wunsch and Heimbach* [2013a]	(1, 0, 1)	[0.06 ± 0.17]	1.81 ± 0.76	[0.53 ± 0.72]	[−0.41 ± 0.76]	0.10 (6)
	AR(1)		0.0	0.78/1.70	0.53		
N	*Allan et al.* [2014]	(1, 0, 1)	[0.08 ± 0.08]	0.96 ± 0.49	0.86 ± 0.08	−0.54 ± 0.13	0.97 (6)
	AR(1)		0.0	0.42/0.76	0.86		
Q	*Levitus et al.* [2012]	(0, 1, 1)	0.21 ± 0.19	1.15 ± 1.05		−0.39 ± 0.23	0.26 (4)
	ARIMA(0, 1, 0)		0.0	1.00/0.45			
Q	*Ishii and Kimoto* [2009]	(0, 1, 1)	0.19 ± 0.18	1.05 ± 0.96		−0.31 ± 0.22	0.41 (5)
	ARIMA(0, 1, 0)		0.0	0.93/0.33			
		(p, d, q)	a (mm)	σ (mm)	ϕ	θ	p-LBQ
M_G	*Box and Colgan* [2013]	(1, 0, 1)	[0.01 ± 0.02]	0.22 ± 0.14	0.95 ± 0.08	−0.54 ± 0.17	0.94 (5)
	AR(1)		0.0	0.10/0.17	0.95		
M_G	*Hanna et al.* [2011]	(1, 0, 1)	[0.00 ± 0.01]	0.27 ± 0.18	0.99 ± 0.31	−0.86 ± 0.18	0.36 (5)
	AR(1)		0.0	0.04/0.26	0.99		
M_{IC}	*Marzeion et al.* [2012]	(1, 0, 1)	[0.010 ± 0.13]	0.48 ± 0.25	0.91 ± 0.11	−0.60 ± 0.24	0.46 (5)
	AR(1)		0.0	0.19/0.39	0.91		
	No Greenland	(1, 0, 1)	[0.10 ± 0.14]	0.35 ± 0.21	0.88 ± 0.16	−0.68 ± 0.25	0.55 (5)
	AR(1)		0.0	0.11/0.31	0.88		
h_T	*Levitus et al.* [2012]	(0, 1, 1)	[0.35 ± 0.37]	1.99 ± 1.76		−0.28 ± 0.24	0.71 (4)
	ARIMA(0, 1, 0)		0.0	1.79/0.56			
h	*Church and White* [2011][d]	(1, 1, 2)	0.044 ± 0.014	7.27 ± 3.03	0.75 ± 0.06	{−1.37 0.39}	0.67 (7)
h	*Jevrejeva et al.* [2006][d]	(1, 1, 2)	[0.036 ± 0.046]	1.54 ± 0.51[e]	0.75 ± 0.10	{−0.41 −0.08}	0.57 (7)

[a]Values in square brackets are not statistically significant.
[b]In the rows for the ARIMA+noise model, values are for $\sigma_\epsilon/\sigma_\xi$.
[c]p value of the Ljung-Box Q-test for residual correlation and the number in parenthesis is the number of lags considered, which is $\sim\ln(N)$ *with* N the sample size.
[d]In both cases, only the homogeneous part of the reconstruction is used; see text for details.
[e]The smaller value of σ in *Jevrejeva et al.* [2006] is due to the fact that the reconstruction uses the mean annual trend for each month, i.e., has units of mm/yr as opposed to *Church and White* [2011] which is in mm/month.

range of time scales [e.g., *Cuffey and Paterson*, 2010; *Cronin*, 2011], and as a consequence, the flux of fresh water from land ice will have persistence over long periods of time. An important consequence of the low frequency variability and the relatively short time series available is the difficulty of distinguishing trends and other nonstationarities, that are externally forced, from internal variability of the atmosphere-ocean-cryosphere coupled system in which low frequency variability may appear as trend-like behavior.

3.2.1. Greenland

For Greenland, total mass balance can be summarized as [*Box and Colgan*, 2013; *Bamber et al.*, 2012]

$$MB = SMB - L_M = A - (R + L_M) \tag{6}$$

where MB is total mass balance, SMB is surface mass balance, L_M is marine ice loss, A is snow accumulation, and R is runoff.

Both runoff and snow accumulation show interannual to interdecadal variability in the reconstructions of *Hanna et al.* [2011] and *Box* [2013] in the period 1840–2010, consistent with a random process with memory. *Box et al.* [2012] extend the accumulation reconstruction back to 1600 and *Andersen et al.* [2006] to 200 A.D., both showing variability on a centennial time scale and no long-term trend. In turn, L_M can be parametrized as a function of either SMB or runoff [*Rignot et al.*, 2008; *Box and Colgan*, 2013], which suggests total MB will exhibit multidecadal to centennial variability similar to SMB. All these suggest the possibility that Greenland's MB can be described by a random process with persistence on decadal to centennial time scales.

The Greenland MB reconstructions of *Box and Colgan* [2013] and *Hanna et al.* [2011], shown in Figure 2, share similar spectral characteristics, with interannual to interdecadal variability, statistically zero mean and lag-1 autocorrelation of 0.65 and 0.52, respectively. Both reconstructions have a SDF that grows with decreasing frequency and shows no clear signs of flattening on time scales of ∼60–100 years. The simplest model that describes both MB reconstructions is an ARMA(1, 1) with no significant drift, which suggests an underlying AR(1) process with added white noise (see Table 4). The AR coefficient $\hat{\phi}$ in both cases exceeds 0.9,

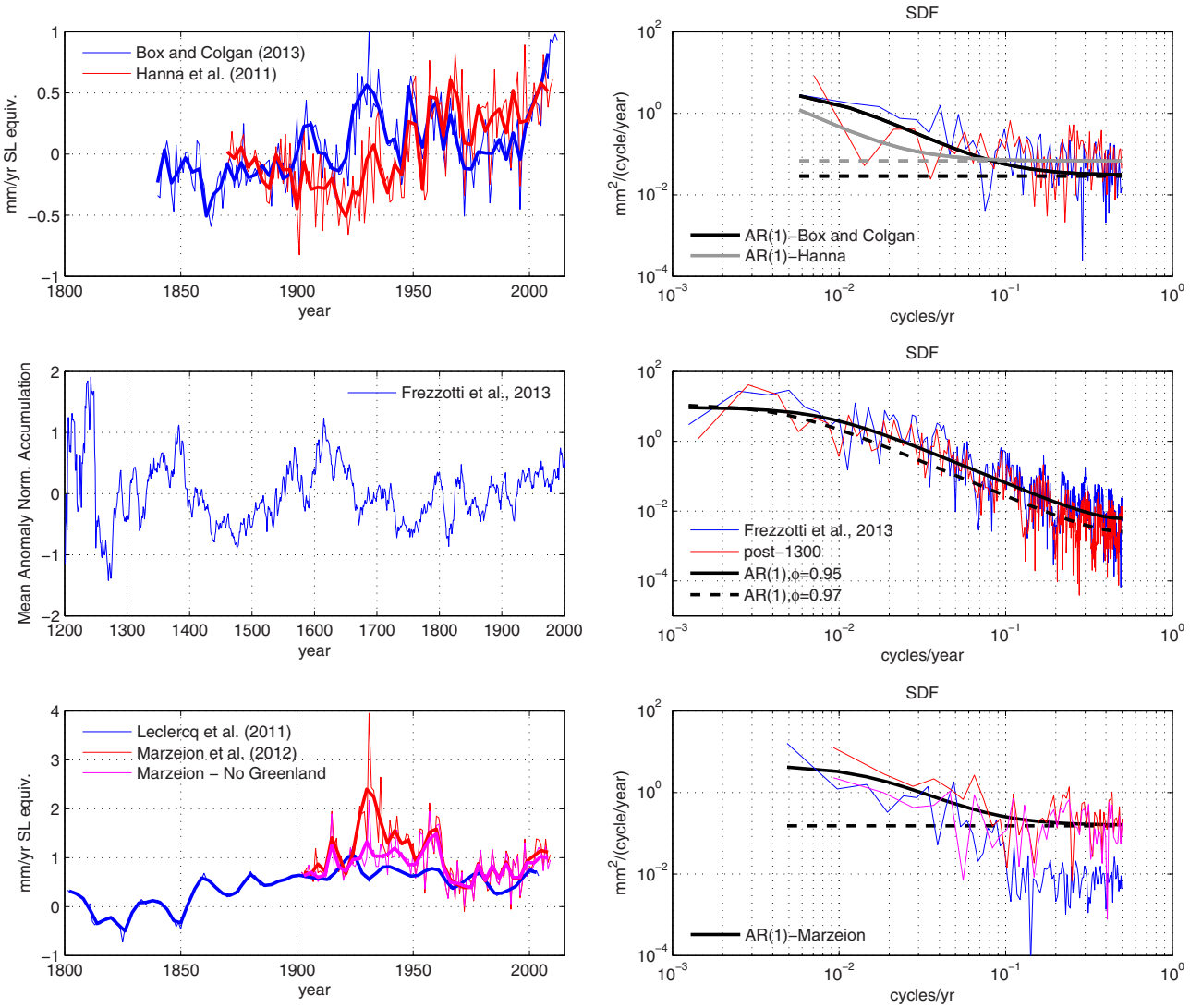

Figure 2. Sea level contributions from (top) glaciers (M_{IC}) estimated by *Leclercq et al.* [2011] and *Marzeion et al.* [2012], (bottom) Greenland (M_G) by *Box and Colgan* [2013] and *Hanna et al.* [2011] and (middle) accumulation over Antarctica estimated by *Frezzotti et al.* [2013]. Notice the different vertical scales in the left column. The right column displays the estimated periodogram (thin lines) together with the theoretical spectra of the fitted ARIMA models (thick lines).

considerably higher than the sample lag-1 autocorrelation, as would be expected from the additive error/reconstruction noise degenerating the underlying AR process.

3.2.2. Antarctica

SMB estimates in Antarctica have no trend over the past 800 years, showing significant variability on time scales from years to centuries [*Frezzotti et al.*, 2013]. *Steig et al.* [2013], using $\delta^{18}O$, also show similar variability in snow melt and temperature in West Antarctica over the last two millennia and link it to decadal atmospheric variability originating in the tropics. *Wingham et al.* [2006] and *Davis et al.* [2005] show that snowfall over East Antarctica in the last few decades might lead to a net mass gain and a mitigation of sea level rise. *Payne et al.* [2004], *Pritchard et al.* [2012], and *Rignot et al.* [2013] propose basal melting, through wind-driven warm water intrusion, as the main cause of mass loss in Antarctica in the last decade. All these mechanisms are consistent with the hypothesis of Antarctic MB having variability on time scales of years to centuries, originating from the interaction/forcing with atmospheric and ocean processes that may be described by (stationary) random processes.

Unfortunately, the authors are not aware of any current reconstruction of Antarctic MB that would allow a test of this hypothesis for M_A. The continental-scale SMB reconstruction from *Frezzotti et al.* [2013], Figure 2, has constant sign in periods extending over a century, trend-like behavior on centennial time scales and

the SDF shows the typical shape of a red noise process, with power increasing with decreasing frequency up to time scales of a century or more. An AR(1) process reproduces these characteristics accurately. Since SMB is closely related to total MB, one would expect similar behavior in the latter with variability on (at least) multidecadal to centennial time scales, that may be the result of a stationary random process.

3.2.3. Glaciers and Ice Caps

Mass balance of individual glaciers is the sum of all accumulation and ablation processes, which in turn are directly linked to atmospheric circulation and changes in corresponding local meteorology (precipitation and temperature) and influenced by topography [e.g., IPCC-AR5, *Cuffey and Paterson*, 2010; *Cronin*, 2011; *Burke and Roe*, 2013]. An important characteristic of individual glaciers/regions, is that they can exhibit kilometer-scale, century-scale fluctuations in glacier length (which is a proxy for glacier mass) in a constant climate [*Burke and Roe*, 2013; *Roe*, 2011; *Roe and O'Neal*, 2009], producing changes similar in magnitude to those attributed to a global Little Ice Age.

Figure 2 shows two of the longest reconstructions available of glacier contribution to GMSL, by *Leclercq et al*. [2011] and *Marzeion et al*. [2012]. While differences in detail are conspicuous, both reconstructions show a negative mass balance starting as far back as the late 1800s, and positive or zero mass balance during the nineteenth century. Furthermore, both reconstructions show multidecadal variability, with a higher mass loss values during the first half of the twentieth century ($\sim$60 years) than afterwards when global atmospheric temperatures are highest (the mean of the first half of *Marzeion et al*. [2012] is twice as large as the second half, 1.31 ± 0.16 versus 0.73 ± 0.11 mm/yr), slowly varying over time and with considerable interannual variability. The SDF of both estimates are similar on time scales longer than $\sim$10 years (the smaller values of *Leclercq et al*. [2011] at high frequencies are caused by the 30 year smoothing used in their reconstruction and has no physical meaning) and increase with decreasing frequency.

The simplest model that describes *Marzeion et al*. [2012] is an ARMA(1, 1) with no significant drift and AR coefficient $\hat{\phi}=0.91$, which suggests an AR(1) with additive error noise. These values remain almost unchanged if Greenland glaciers are excluded from *Marzeion et al*. [2012], which account for the major differences with *Leclercq et al*. [2011]. This latter reconstruction is more difficult to analyze in terms of an ARIMA model, because the reconstruction method includes a 30 year moving average that heavily distorts the autocorrelation function, and in practice renders the ARIMA fitting exercise of little use.

4. Analysis of GMSL Reconstructions

4.1. Characterization of GMSL Reconstructions as Integrated Processes

All reconstructions have a power law SDF with exponent ~ -2 on time scales from a few years (3–5) up to the length of the reconstructions of 130–300 years (see Figure 3 and Table 3). One possible explanation for the power law form is a deterministic trend in the time series [e.g., *Percival and Walden*, 1993]. This cannot be the only cause, since the power law form of the spectrum at low frequencies remains after subtracting a linear trend (or even a quadratic one) from the reconstructions. This fact strongly suggests the possibility of the reconstructions being integrated processes.

The integrated character of the GMSL reconstructions is consistent with the results of two different statistical tests routinely used in the literature [e.g., *Schmith et al*., 2012; *Barbosa*, 2011; *Fatichi et al*., 2009; *Wu et al*., 2007; *Percival et al*., 2001; *Pierce*, 2001] (see Appendix B2), the Kwiatkowski-Phillips-Schmidt-Shin test (KPSS) [*Kwiatkowski et al*., 1992] for trend stationarity and the Phillips-Perron test (PP) [*Phillips and Perron*, 1988] for the presence of a unit root. In JM, JE, and C11, both tests deliver consistent results, with KPSS rejecting the null hypothesis at the 99% confidence level, and PP failing to do so, strongly suggesting the possibility that the reconstructions are integrated processes. In contrast, in CM (even considering only the post-1930 period), KPSS and PP reject their respective null hypotheses of trend stationarity and integrated process, both at the 99% confidence level. This result indicates that either the tests are not powerful enough or CM is inappropriate to characterize the reconstruction as either integrated or trend stationary.

4.2. ARIMA Model

Following *Box et al*. [2008], the value of d for an integrated process can be derived from the series of differences $\Delta^d h(t)$. In all reconstructions, $\Delta h(t)$ is normally distributed (the exception is JE if the whole

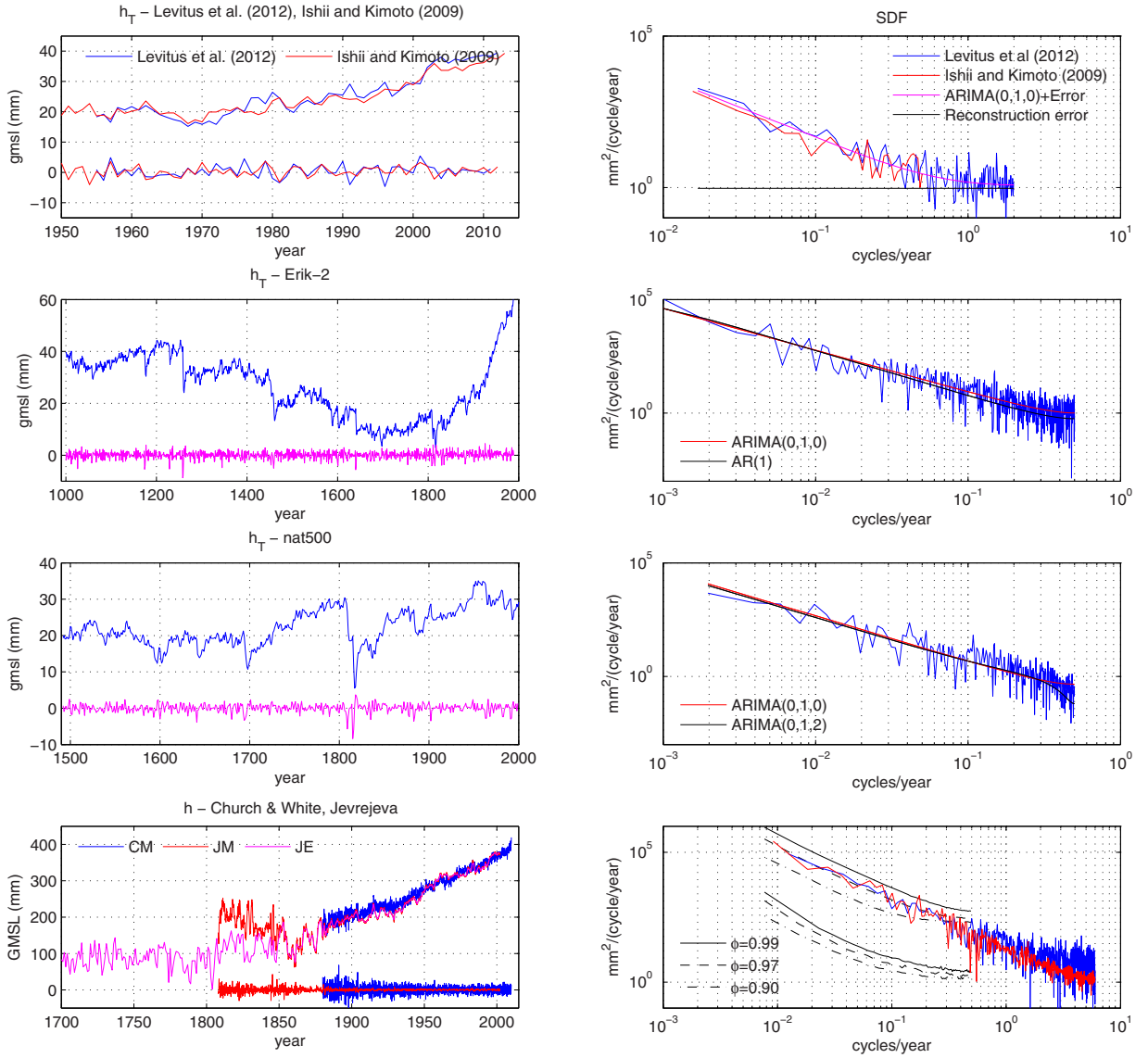

Figure 3. (top) Thermosteric sea level (h_T) estimated by *Levitus et al.* [2012] and *Ishii and Kimoto* [2009] and (middle) derived from AOGCM simulations Erik-2 and nat500, along with their SDF. Also shown in the left column are the series of first differences $\Delta h_T(t)$. (bottom row) Sea level reconstructions by *Church and White* [2011] (CM), *Jevrejeva et al.* [2006] (JM), and *Jevrejeva et al.* [2008]. The spectra are calculated using only the homogeneous part of the reconstructions (see text). The black curves are the 95% confidence intervals estimated with the ensemble of synthetic series for different values of ϕ_M (see equation (8)).

reconstruction period is considered) and has no significant linear trend, indicating stationarity and hence $d = 1$ (Table 3 and Figure 3). This value of $d = 1$ is consistent with the form of the SDF and the value of d_e.

The autocorrelation function of $\Delta h(t)$ in CM is characterized by a negative value of ~ -0.4 at lag 1 and zero otherwise, whereas JM has small values between 0.36 and 0.17 at the first few lags and -0.4 at lag 12, resulting from the reconstruction method used in *Jevrejeva et al.* [2006], which "calculate the mean annual rate for a given month over a whole year (e.g., the rate in January is calculated as the July to July difference)." This procedure is equivalent to using a 12 month running mean on $\Delta h(t)$, which introduces spurious correlation and distorts the existing correlation [see *Foster and Brown*, 2015]. For this reason, while an ARIMA model can be fitted to the reconstructed GMSL values, its interpretation in terms of $\hat{h}(t)$ and $\zeta(t)$ is less obvious.

The simplest model for the reconstructions is an ARIMA(1, 1, 2), which gives similar parameter values for both reconstructions (see Table 4), in particular a value of $\hat{\phi} = 0.75$, indicating a process that integrates red

noise. The value of the drift a is also similar in both reconstructions, at 0.044 ± 0.014 and 0.036 ± 0.046 mm/month for CM and JM, respectively, which corresponds to an exogenously forced linear trend of ~0.53 and ~0.43 mm/yr, smaller than the linear trend obtained by standard regression methods. In JM, the value of the drift is statistically not different from zero. An ARIMA(1, 1, 3) (not shown in Table 4) produces almost identical results except for a slightly higher value of $\phi = 0.77$ and smaller $a = 0.039 \pm 0.013$ mm/month in CM.

The ARIMA(1, 1, n) with $n = 1, 2$ suggests an underlying ARIMA(1, 1, 0) embedded in white or MA(1)-noise respectively, but the process with parameters ϕ, θ_i, and σ estimated with our time series cannot be represented by the addition of an ARIMA(1, 1, 0) and added white or MA(1)-noise. This can be due to $\Delta\hat{h}(t)$ having a different structure than an AR(1) process, as is expected from the fact that $\hat{h}(t)$ is the addition of several processes with different spectral characteristics (i.e., thermal expansion and fresh water flux). An alternative explanation is the fact that the ARIMA(1, 1, 0) embedded in white or MA(1)-noise model does not allow for the possibility of reconstruction noise added to $\Delta h(t)$ (rather than only to $h(t)$), as is the case in CM and JM, nor for the possibility of reconstruction errors with a more complex structure, as can be expected from the reconstruction methods (see section 2.1).

5. Synthetic Time Series

Using the random walk and AR(1) models derived for $F(t)$ and $M(t)$ in section 3, we construct a $N_m = 10{,}000$ member ensemble of synthetic time series of length N_t between 130 (the length of the *Church and White* [2011] reconstruction) and 1000 years:

$$\bar{h}_i(t) = \Psi_i(t) + \sum_{t'=1}^{t} (\lambda\bar{F}_i(t') + \bar{M}_i(t'))\Delta t \qquad t = 1, \ldots, N_t \qquad i = 1, \ldots, N_m$$
$$\lambda\bar{F}_i(t) = \epsilon_F \tag{7}$$
$$\bar{M}_i(t) = \phi_M \bar{M}_i(t-1) + \epsilon_M$$

where $\Delta t = 1$ year, $\lambda\bar{F}_i(t)$ is white noise representing the thermal expansion of the ocean, with $\sigma_{\epsilon_F} = 1.8$ mm (Table 4); $\bar{M}_i(t)$ is an AR(1) process representing the fresh water flux from land ice masses, with $\phi_M = 0.99$ (0.90) and $\sigma_{\epsilon_M} = 0.25$ mm (Table 4); and Ψ_i is a white noise process representing the reconstruction errors, with $\sigma_\Psi = 5$ mm, which is a low estimate of the value for the GMSL $1-\sigma$ error in *Church and White* [2011] or *Jevrejeva et al.* [2008]. The value of ϕ_M is chosen taking into account that the lag-1 autocorrelation estimate for an AR(1) process with coefficient ϕ, with a sample size N_t, has an approximate bias of $-\frac{1+4\phi}{N_t}$ [*Storch and Zwiers*, 1999], which for $\phi = 0.99$ and $N_t = 130$ is ~ -0.04. The mean of the ϕ values estimated for M_G and M_{IC} is 0.95, suggesting a value $\phi_M \sim 0.95 + 0.04 = 0.99$. We take this value as an upper bound, and we also test the results with a central value of $\phi_M = 0.97$ and a lower bound of $\phi_M = 0.90$ to cover a plausible range. The value of σ_{ϵ_M} reflects the assumption that $\bar{M}(t)$ is the sum of three independent identical AR(1) processes (M_G, M_A, and M_{IC}).

This model reproduces the statistics of both C11 and JE accurately for $N = 130$ and $\phi_M = 0.99$ (0.97) (confidence intervals are at the 95% level): the mean value of $\Delta\bar{h}(t)$ is 0.01 ± 2.13 (0.00 ± 1.23) mm versus 1.65 and 1.73 mm in C11 and JE, respectively; the standard deviation is 7.35 ± 1.07 (7.35 ± 1.08) mm versus 5.71 and 8.41 mm; and the lag-1 autocorrelation -0.44 ± 0.13 (-0.44 ± 0.13) versus -0.28 and -0.24. The values of standard deviation and lag-1 autocorrelation are highly dependent on the model chosen for $\Psi_i(t)$, which in our case is assumed to be white noise, but even a weakly autocorrelated process delivers values for $\Delta\bar{h}(t)$ closer to C11 and JE. The linear trend in $\bar{h}(t)$ over the full 130 year period, calculated with linear regression, is 0.01 ± 2.32 (0.01 ± 1.33) mm/yr versus 1.54 and 1.74 mm/yr.

Figure 4 shows the envelope created by the members of the ensemble for values of ϕ_M of 0.99, 0.97, and 0.90, together with C11 and JE. Also shown are the 99, 95, and 90 percentiles of the linear trends on time scales between 10 and 1000 years. For $\phi_M = 0.99$, both reconstructions are within 90% of the ensemble members and the linear trends of C11 and JE in the period 1880–2011 fall well below the 90 percentile of ~2 mm/yr. For $\phi_M = 0.97$, linear trends of both reconstructions fall between the 99 and 95 percentiles, whereas for $\phi_M = 0.90$ both fall well above the 99 percentile of ~0.8 mm/yr. This results show the sensitivity of the significance of the GMSL trend in the instrumental record to the low frequency spectral character of

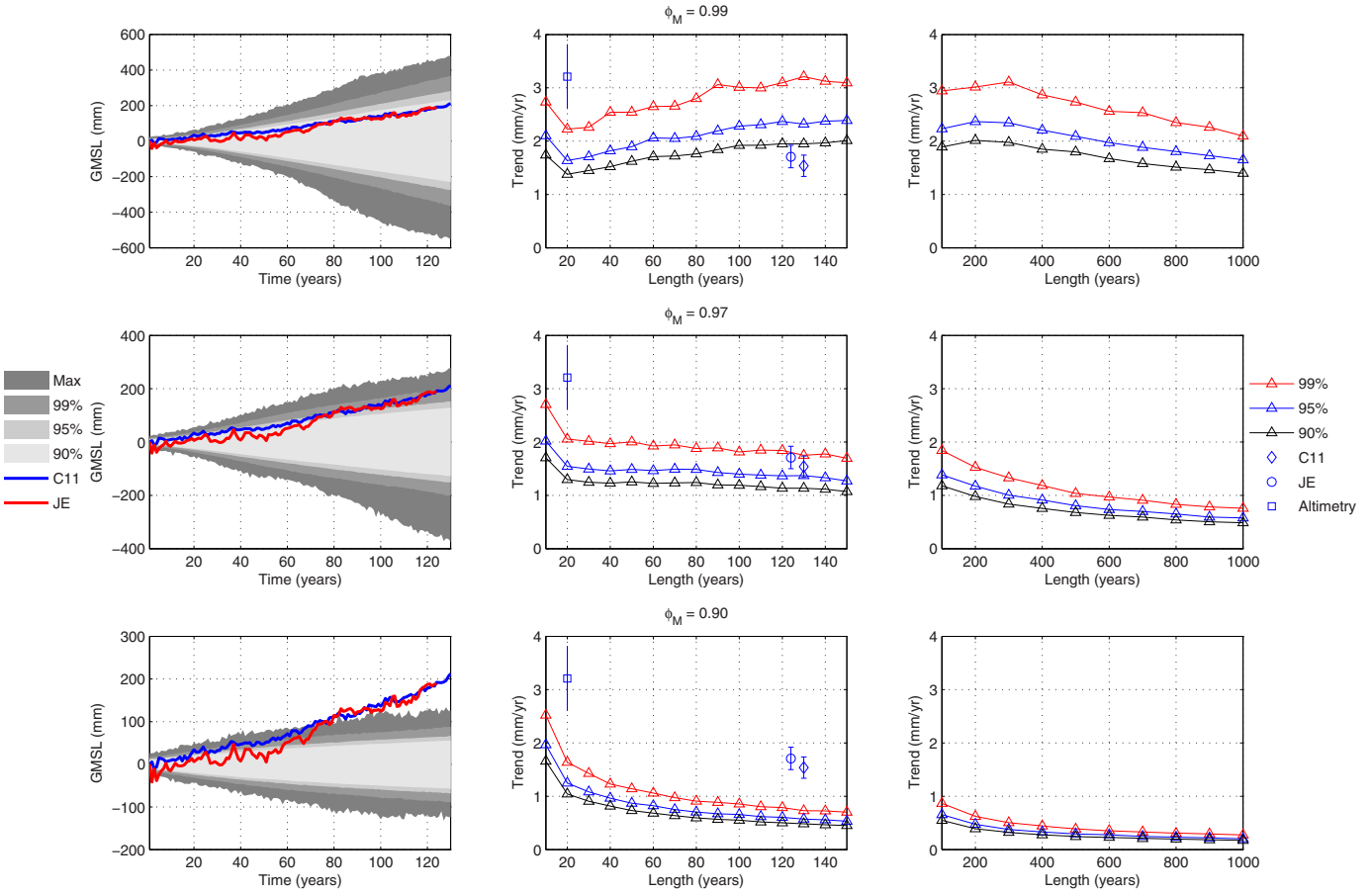

Figure 4. (left column) Envelope of the 10,000 ensemble members of synthetic sea level. Each row corresponds to a different value of ϕ_M, the coefficient of the AR(1) model in equation (8), indicated in the center column. The grey shadings indicate the maximum range and the limits of different percentiles. Year 1 corresponds to 1880. Middle and right columns: 99, 95, and 90 percentiles of the linear trends versus length of the interval over which the trend is calculated, from 1 to 1000 years. Also shown are the values of the trends for the *Church and White* [2011] and *Jevrejeva et al.* [2008] for the period 1880–2011 and their respective 95% confidence intervals.

$M(t)$, which may show natural variability on time scales of several centuries, much longer than the observational records available. Even for the low estimate $\phi_M = 0.90$ the 95% interval of 200 year trends is 0.6 mm/yr, and for 2000 year trends (not shown) is 0.1 mm/yr. The corresponding values for $\phi_M = 0.99/0.97$ are 2.2/1.1 and 1.0/0.3 mm/yr, respectively, comparable to the IPCC-AR5 estimate of a few tenths of a mm/yr averaged over the last 2 kyr, and ± 0.25 m on time scales of a few hundred years. Figure 3 shows the 95% confidence intervals for different values of ϕ_M, which exhibit a pattern similar to the linear trends, with SDF of both reconstructions well within the interval for $\phi_M = 0.99$ and outside of it for $\phi_M = 0.90$.

6. Conclusion

While it is unlikely that the whole of the GMSL rise in the instrumental record is caused by natural variability alone, our analysis shows that the GMSL reconstructions available are consistent with sea level rise being an integrated process with natural variability on centennial time scales. The integrated character is a direct consequence of the fact that GMSL is the result of a cumulative process, and is consistent with present estimates of both thermosteric sea level rise and changes in the mass balance of land ice masses. Furthermore, the underlying physical processes associated with GMSL rise suggest and are consistent with, the possibility of century-scale fluctuations in GMSL even in a "constant climate," produced by the integration of random variations that are zero mean and stationary. Internal variability and externally forced sea level changes (e.g., through anthropogenic influence) together form the full spectrum of GMSL variability observed.

We have presented a simple model of centennial to millennial natural variability of GMSL that is physically plausible, parsimonious and describes accurately the reconstructed time series of *F*, *M*, and GMSL. This

model indicates that the sum of zero mean stationary low-order autoregressive processes, which are the simplest representation of geophysical processes with memory (without making explicit reference to the underlying physical processes), and reconstruction errors (ubiquitous in measurements and reconstructions of GMSL and its components), is capable of producing centennial to millennial variability with the same characteristics as the exhibited by GMSL reconstructions. This allows to construct a model for GMSL, tested by the use of synthetic time series, and use well calibrated statistics to infer detection levels of deterministic trends. In this way, the present contribution complements the existing body of work trying to understand observed variability of GMSL and its relation to stochastic processes.

Reconstruction errors may introduce inhomogeneities and spurious trends on time scales as long as the reconstruction period itself. This severely affects the estimation of parameters of any model fitted to the reconstructions, and must be taken into account when exploring the possible causes behind GMSL variability. Furthermore, variability on time scales of months to a few years is paramount to explain the long-term trends and multidecadal variability observed in F, M, and GMSL, and the latter cannot be explained without the former. This is due to the long persistence processes in land ice masses and the integrated character of $h_T(t)$ and $h_E(t)$. The high values of the coefficient ϕ in the estimated AR(1) models that describe $M(t)$ (section 3), strongly point to the need of long time series, not available at present, that allow for the study of low frequency variability, and to the difficulties of interpreting trend-like behavior in short observational records. Whether the GMSL trend observed in the instrumental record, or what part thereof, can be attributed to natural variability and what part is forced externally, e.g., through anthropogenic influence on the climate, depends critically on the value of ϕ, i.e. on the low frequency spectral characteristics of $h_E(t)$.

The presence of internal variability of GMSL variations on time scales of several decades to centuries may be an important factor in some unresolved questions such as the causes of the apparent onset of the present quasi-linear GMSL rise since the late nineteenth century, the presence or absence of GMSL variability in the last 2–3 kyr or the presence of an acceleration in the period covered by the instrumental record. Furthermore, the integrated character of GMSL causes an inherent difficulty in distinguishing natural variability from externally forced changes, since both are integrated by the ocean. These characteristics may compromise the value of GMSL as a "climate indicator" unless one is able to characterize fully one or both of these contributions. Similar results have been found for other climate processes thought to be good indicators of climate change, e.g. the Atlantic Meridional Overturning Circulation (AMOC) [*Wunsch and Heimbach*, 2013b], the North Atlantic Oscillation (NAO) [*Percival et al*., 2001; *Wunsch*, 1999], or the Atlantic Multidecadal Oscillation (AMO) [*Clement et al*., 2015]. Similarly, future projections of GMSL rise will be affected by the integrated character of GMSL.

This study aims at a characterization of the possibility of significant natural variability of GMSL on centennial time scales, rather than a precise description of GMSL and its dynamics, and much work remains to be done to fully describe the causes and modes of sea level variability, as well as the influence of external forcing factors. Future work needs to include the physical processes involved in the dynamics of GMSL, especially the reduction of uncertainties in estimates of the GMSL contribution from land ice masses. Attention should turn to detailed spatiotemporal patterns of sea level change, as observed by the satellite altimetric record (now exceeding 20 years) that enable more detailed dynamical interpretation of the observed signal. The details offered by the altimetric data mandate the continuation of an uninterrupted altimetric time series in the foreseeable future.

Appendix A: A Linear Approximation to a Physical Model of Global Mean Sea Level

Even though h_T and h_E are not strictly independent of each other, on centennial time scales and at the basic level of explanation of the model proposed, we consider the assumption of independence appropriate. It is commonplace in the literature, and GMSL is considered as the simple addition of the individual contributions from individual land ice masses and the thermal expansion of the ocean [e.g., *Stocker et al*., 2013; *Church and White*, 2011].

At first order, the change in ocean volume ΔV over time Δt implied by heat flux F is given by the equation of state

$$\frac{\Delta V}{V} = \alpha \Delta T = \frac{\alpha}{c_p} \frac{F \Delta t}{\rho V} \tag{A1}$$

where α is the coefficient of thermal expansion, c_p is the specific heat capacity (at constant pressure), and ρ the density of sea water. As an approximation, both density and specific heat capacity can be considered

independent of temperature and pressure, i.e., c_p,ρ = constant (but see *Griffies and Greatbatch* [2012] for an extensive discussion of higher-order effects). The change in volume is due to the change in height of the water column, so that $\Delta V = A_{oc}\Delta h_T$, with A_{oc} the area of the ocean. Rearranging terms in equation (A1) we obtain

$$\frac{\Delta h_T}{\Delta t} = \lambda F \tag{A2}$$

where λ is the "expansion efficiency of heat," which can be considered independent of temperature and pressure for the conditions relevant to our problem, and hence a constant independent of current GMSL for the global ocean [*Russell et al*., 2000]. This implies that the function $f(F) = \lambda F$ is a linear function, as is also proposed by e.g., *Storch et al*. [2008].

Thermal expansion occurs instantaneously, without delay on the time scale Δt, so that the expansion due to a heat pulse $F\Delta t$ takes place completely within the interval Δt. For the mixed layer (or even down to 700 m depth, for which longer data time series are available and where most of the expansion observed takes place), in a time interval $\Delta t = 1$ to 3 moths (or even a year) heat fluxes of the magnitude observed are completely absorbed and mixed. Notice that with the assumption of constant ρ, this approximation holds automatically regardless of the value of Δt.

$\dot{h}_E$ is simply the change in sea level due to the addition of mass in the form of fresh water and hence $g(M) = \beta M$ is a linear function. Since β is simply a conversion factor from ice mass balance (in units of Gt of water) to mm of GMSL equivalent, it is constant and independent of h_E and the barystatic contribution to GMSL is

$$\frac{\Delta h_E}{\Delta t} = \beta M \tag{A3}$$

Changes in sea level occur instantaneously following the addition of melt water, since we are considering only GMSL and not its regional distribution. We also ignore the possible effect of isostatic rebound following melting of ice masses. Furthermore, the fresh water flux into the ocean is independent of current sea level $h_E(t)$.

Appendix B: Statistical Models and Methods

The ARIMA model equation (4) without added errors can be expanded as

$$\left(1-\sum_{i=1}^{p}\phi_i B^i\right)(1-B)^d x(t) = a+\left(1+\sum_{i=1}^{q}\theta_i B^i\right)\epsilon(t) \tag{B1}$$

Equation (B1) includes several models widely used in the geosciences community. In particular, for $d = 1$, which is the main focus of this study, we can write equation (B1) in the more explicit (and familiar) form

$$\Delta x(t) = a+\phi_1\Delta x(t-1)+\ldots+\phi_p\Delta x(t-p)+\epsilon(t)+\theta_1\epsilon(t-1)+\ldots+\theta_q\epsilon(t-q) \tag{B2}$$

where $\Delta x(t) = (1-B)x(t) = x(t)-x(t-1)$. In the absence of a constant term ($a = 0$) and for $p = q = 0$, equation (B2) reduces to a pure random walk in which $x(t+1) = x(t)+\epsilon(t+1)$ is the cumulative sum of pure white noise and is an $I(1)$. For $d = q = 0$, we obtain an autoregressive process of order p, AR(p), in which the system has memory of past values up to p previous time steps (for instance, if $p = 1$ we obtain the well-known AR(1) process $x(t+1) = \phi x(t)+\epsilon(t+1)$). Finally, $d = p = 0$ gives a moving average process of order q, MA(q), in which the system has memory of past random shocks $\epsilon(t)$ up to q previous time steps, $x(t) = \epsilon(t)+\sum_{i=1}^{q}\theta_i\epsilon(t-i)$.

The spectral density function (SDF) of the ARIMA process with added noise and $a = 0$, under the assumption that $\zeta(t)$ and $\hat{x}(t)$ are independent of each other, can be expressed as [*Palma*, 2007]

$$\Phi(\omega) = \frac{\sigma_\epsilon^2}{2\pi}[2\sin(\omega/2)]^{-2d}\frac{|\hat{\theta}(e^{-i\omega})|^2}{|\hat{\phi}(e^{-i\omega})|^2}+\frac{\sigma_\zeta^2}{2\pi}\frac{|\tilde{\theta}(e^{-i\omega})|^2}{|\tilde{\phi}(e^{-i\omega})|^2} \tag{B3}$$

which has a pole at $\omega = 0$. If $\zeta(t)$ can be represented by a stationary random process, the SDF of $x(t)$ at low frequencies can be approximated by the SDF of $\hat{x}(t)$ and the effect of the reconstruction errors is negligible. This is the basis of our spectral analysis, which is based in the low frequency part of the SDF and assumes that a these low frequencies the SDF of $x(t)$ is dominated by that of $\hat{x}(t)$.

B1. Equivalence Between ARIMA and ARIMA With Added Noise Models

We refer the reader to *Granger and Morris* [1976] and *Box et al*. [2008] for a complete derivation of the following results. Consider first the equivalence of an AR(1) with added white noise and an ARMA(1, 1). Let $(1+\phi B)x_t=\epsilon_t$ be an AR(1) process, $y_t=\eta_t$ a white noise process, and their sum $z_t=x_t+y_t$ (where t is time). The latter is an ARMA(1, 1) given by

$$(1+\phi B)z_t=(1+\phi B)\eta_t+\epsilon_t \tag{B4}$$

For an ARMA(1, 1) process, $(1+\gamma B)z_t=(1+\theta B)\zeta$ to be equivalent, the variance κ_0 and first autocovariance κ_1 of both process have to be equal (all autocovariances for lags ≥ 1 are zero in a MA(1)). One has

$$\begin{gathered}\phi=\gamma\\ \kappa_0=(1+\theta^2)\sigma_\zeta^2=(1+\phi^2)\sigma_\eta^2+\sigma_\epsilon^2\\ \kappa_1=\theta\sigma_\zeta^2=\phi\sigma_\eta^2\end{gathered}$$

This system of equations can be solved to obtain

$$\begin{gathered}\sigma_\epsilon^2=\sigma_\zeta^2\left(1+\theta^2-\frac{\theta}{\phi}(1+\phi^2)\right)\\ \sigma_\eta^2=\frac{\theta}{\phi}\sigma_\theta^2\end{gathered} \tag{B5}$$

where the values of γ, θ, and σ_ζ^2 are obtained fitting an ARMA(1, 1) to the time series $z(t)$.

The equivalence between an ARIMA(0, 1, 1) and an ARIMA(0, 1, 0) (a random walk) with added white noise can be reduced to the previous case. Consider the ARIMA(0, 1, 0) process $X_t=\sum_{i=1}^{t}x_t$ where $x_t=\epsilon_t$ is white noise, the white noise process $Y_t=\eta_t$ and their sum $Z_t=X_t+Y_t$. By taking first differences we obtain $\Delta Z_t=z_t$ and

$$z_t=x_t+\Delta Y_t=\epsilon_t+(1-B)\eta_t \tag{B6}$$

For this process to be equivalent to a MA(1) $z_t=(1+\theta B)\zeta_t$, the autocovariances have to be equal and we obtain

$$\begin{gathered}\sigma_\epsilon^2=(1+\theta+\theta^2)\sigma_\zeta^2\\ \sigma_\eta^2=-\theta\sigma_\zeta^2\end{gathered} \tag{B7}$$

An alternative expression as a function of the lag one autocorrelation of ΔZ_t is $\sigma_\epsilon^2=\sigma_z^2(1+2\rho_z)$.

The equivalence between an ARIMA(1, 1, 0) with noise and an ARIMA(1, 1, n) with $n=2, 3$ can be derived in a similar form, starting with an integrated process $Z_t=X_t+Y_t$, the sum of an AR(1) and a noise process and taking first differences.

B2. Statistical Tests

The evaluation of the skill of the models in describing the time series to which they are fitted requires some choice in the part of the modeler. It is a compromise between the physical soundness of the statistical model, parsimony and goodness of fit. The latter is quantified with the Ljung-Box Q-test for residual correlation (LBQ) [*Box et al*., 2008]. In addition to the LBQ test, which is not always applicable, the periodogram of the time series is compared with the theoretical spectrum predicted by the fitted model. In this context, a model represents well the data if: it is the most parsimonious model compatible with the physical processes underlying the time series; describes well its spectrum, especially at low frequencies (several decades to centuries); gives the highest possible p value of the LBQ test subject to the two previous conditions.

The integrated character of a time series is evaluated with two complementary tests. The Kwiatkowski-Phillips-Schmidt-Shin test (KPSS) [*Kwiatkowski et al*., 1992] uses the model

$$\begin{gathered}x(t)=c(t)+kt+\epsilon_1(t)\\ c(t+1)=c(t)+\epsilon_2(t)\end{gathered}$$

where k is a constant, $\epsilon_1(t)$ is a stationary random process, and $\epsilon_2(t)$ is a zero mean independent identically distributed process with variance σ_2^2. The null hypothesis is $\sigma_2^2=0$ so that c is a constant intercept in the model, against the alternative $\sigma_2^2\neq 0$ so that $c(t)$ is a random walk.

The Phillips-Perron test (PP) [*Phillips and Perron*, 1988] tests the null model

$$x(t)=c+x(t-1)+\epsilon(t)$$

where c is a constant and $\epsilon(t)$ is a stationary random process, against the alternative

$$x(t)=c+kt+\phi x(t-1)+\epsilon(t)$$

where c and k are constants, $\epsilon(t)$ is a stationary random process, and $\phi < 1$. Both test statistics require that a number of lags is specified for the Newey-West estimate of long run variance. In KPSS, the number of lags is $\sim\sqrt{N}$ as suggested by *Kwiatkowski et al.* [1992], whereas in PP is $\sim N^{\frac{1}{4}}$ [*Phillips and Perron*, 1988], where N is the sample size.

Acknowledgments

Radiative balance at the TOA data from *Allan et al.* [2014] are available at http://www.met.reading.ac.uk/sgs02rpa/research/DEEP-C/GRL/. Heat content and thermosteric sea level data from *Levitus et al.* [2012] are available at http://www.nodc.noaa.gov/OC5/3M_HEAT_CONTENT/index.html. The data files are heat_content_anomaly_0-700_seasonal.nc; heat_content_anomaly_0-700_yearly.nc; mean_thermosteric_sea_level_anomaly_0-700_seasonal.nc; mean_thermosteric_sea_level_anomaly_0-700_yearly.nc. Heat content and thermosteric sea level data from *Ishii and Kimoto* [2009] are available at http://www.data.jma.go.jp/gmd/kaiyou/english/ohc/ohc_global_en.html. Data corresponding to the global mean sea level reconstructions are available from the Permanent Service for Mean Sea Level (PSMSL) at http://www.psmsl.org/products/reconstructions/church_white_grl_gmsl.lis for *Church and White* [2011] (note that this version is calculated using filtered tide gauge station data); http://www.psmsl.org/products/reconstructions/gslJC2006.txt for *Jevrejeva et al.* [2006]; http://www.psmsl.org/products/reconstructions/gslGRL2008.txt for *Jevrejeva et al.* [2008]. Satellite altimetry data were obtained from http://www.cmar.csiro.au/sealevel/sl_data_cmar.html. The series used in this study is in the file: jb_iby_sry_gtn_giy.nc.gz. Other data used in this study were obtained from the authors of the corresponding reconstructions upon request. This study was supported in part through NSF grants 0961713 and 0934404. We thank Jason Box, Edward Hanna, Paul Leclercq, Ben Marzeion, Claudio Scarchilli, and Neil White for making available many of the time series used in this study and for their help with our questions about the data. We thank Hans von Storch for the initial impulse to this work and Carl Wunsch for innumerable discussions and insights. We also thank An T. Nguyen and Eri Saikawa for many fruitful discussions and help.

References

Ablain, M., A. Cazenave, G. Valladeau, and S. Guinehut (2009), A new assessment of the error budget of global mean sea level rate estimated by satellite altimetry over 1993–2008, *Ocean Sci.*, *5*(2), 193–201, doi:10.5194/os-5-193-2009.

Allan, R. P., C. Liu, N. G. Loeb, M. D. Palmer, M. Roberts, D. Smith, and P.-L. Vidale (2014), Changes in global net radiative imbalance 1985–2012, *Geophys. Res. Lett.*, *41*, 5588–5597, doi:10.1002/2014GL060962.

Andersen, K. K., P. D. Ditlevsen, S. O. Rasmussen, H. B. Clausen, B. M. Vinther, S. J. Johnsen, and J. P. Steffensen (2006), Retrieving a common accumulation record from Greenland ice cores for the past 1800 years, *J. Geophys. Res.*, *111*, D15106, doi:10.1029/2005JD006765.

Antonov, J. I., S. Levitus, and T. P. Boyer (2002), Steric sea level variations during 1957–1994: Importance of salinity, *J. Geophys. Res.*, *107*(C12), 8013, doi:10.1029/2001JC000964.

Bamber, J., M. van den Broeke, J. Ettema, J. Lenaerts, and E. Rignot (2012), Recent large increases in freshwater fluxes from Greenland into the north Atlantic, *Geophys. Res. Lett.*, *39*, L19501, doi:10.1029/2012GL052552.

Barbosa, S. M. (2011), Testing for deterministic trends in global sea surface temperature, *J. Clim.*, *24*(10), 2516–2522, doi:10.1175/2010JCLI3877.1.

Becker, M., M. Karpytchev, and S. Lennartz-Sassinek (2014), Long-term sea level trends: Natural or anthropogenic?, *Geophys. Res. Lett.*, *41*, 5571–5580, doi:10.1002/2014GL061027.

Box, G. E. P., G. M. Jenkins, and G. C. Reinsel (2008), *Time Series Analysis: Forecasting and Control, Wiley Ser. Probab. Stat.*, 4th ed., John Wiley & Sons, Inc., Hoboken, N. J.

Box, J. E. (2013), Greenland ice sheet mass balance reconstruction. Part II: Surface mass balance (1840–2010), *J. Clim.*, *26*(18), 6974–6989, doi:10.1175/JCLI-D-12-00518.1.

Box, J. E., and W. Colgan (2013), Greenland ice sheet mass balance reconstruction. Part III: Marine ice loss and total mass balance (1840–2010), *J. Clim.*, *26*, 6990–7002, doi:10.1175/JCLI-D-12-00546.1.

Box, J. E., et al. (2012), Greenland ice sheet mass balance reconstruction. Part I: Net snow accumulation (1600–2009), *J. Clim.*, *26*(11), 3919–3934, doi:10.1175/JCLI-D-12-00373.1.

Burke, E., and G. Roe (2013), The absence of memory in the climatic forcing of glaciers, *Clim. Dyn.*, *42*, 1335–1346.

Chandler, R. E., and M. E. Scott (2011), Stochastic trends, in *Statistical Methods for Trend Detection and Analysis in the Environmental Sciences*, pp. 171–234, John Wiley and sons, Ltd., Chichester, U. K., doi:10.1002/9781119991571.ch5.

Christiansen, B., T. Schmith, and P. Thejll (2010), A surrogate ensemble study of sea level reconstructions, *J. Clim.*, *23*(16), 4306–4326, doi:10.1175/2010JCLI3014.1.

Church, J., and N. White (2011), Sea-level rise from the late 19th to the early 21st century, *Surv. Geophys.*, *32*(4), 585–602, doi:10.1007/s10712-011-9119-1.

Church, J. A., and N. J. White (2006), A 20th century acceleration in global sea-level rise, *Geophys. Res. Lett.*, *33*, L01602, doi:10.1029/2005GL024826.

Church, J. A., D. Monselesan, J. M. Gregory, and B. Marzeion (2013a), Evaluating the ability of process based models to project sea-level change, *Environ. Res. Lett.*, *8*(1), 014051.

Church, J. A., et al. (2013b), Seas level change, in *Climate Change 2013: The Physical Science Basis. Contribution of Working Group I to the Fifth Assessment Report of the IPCC*, Cambridge Univ. Press, N. Y.

Clement, A., K. Bellomo, L. N. Murphy, M. A. Cane, T. Mauritsen, G. Rdel, and B. Stevens (2015), The Atlantic Multidecadal Oscillation without a role for ocean circulation, *Science*, *350*(6258), 320–324.

Cronin, T. M. (2011), Was pre-twentieth century sea level stable?, *Eos Trans. AGU*, *92*(49), 455–456.

Cronin, T. M. (2012), Rapid sea-level rise, *Quat. Sci. Rev.*, *56*(0), 11–30, doi:10.1016/j.quascirev.2012.08.021.

Cuffey, K., and W. Paterson (2010), *The Physics of Glaciers*, Elsevier Sci., Burlington, Mass.

Dangendorf, S., D. Rybski, C. Mudersbach, A. Mller, E. Kaufmann, E. Zorita, and J. Jensen (2014), Evidence for long-term memory in sea level, *Geophys. Res. Lett.*, *41*, 5564–5571, doi:10.1002/2014GL060538.

Davis, C. H., Y. Li, J. R. McConnell, M. M. Frey, and E. Hanna (2005), Snowfall-driven growth in east Antarctic ice sheet mitigates recent sea-level rise, *Science*, *308*(5730), 1898–1901.

Fatichi, S., S. M. Barbosa, E. Caporali, and M. E. Silva (2009), Deterministic versus stochastic trends: Detection and challenges, *J. Geophys. Res.*, *114*, D18121, doi:10.1029/2009JD011960.

Foster, G., and P. Brown (2015), Time and tide: Analysis of sea level time series, *Clim. Dyn.*, *45*(1–2), 291–308.

Fraedrich, K., R. Blender, and X. Zhu (2009), Continuum climate variability: Long-term memory, scaling, and 1/f-noise, *Int. J. Mod. Phys. B*, *23*(28/29), 5403–5416.

Frankignoul, C., and K. Hasselmann (1977), Stochastic climate models, Part II: Application to sea-surface temperature anomalies and thermocline variability, *Tellus, Ser. A*, *29*(4).

Frezzotti, M., C. Scarchilli, S. Becagli, M. Proposito, and S. Urbini (2013), A synthesis of the Antarctic surface mass balance during the last 800 yr, *Cryosphere*, *7*(1), 303–319, doi:10.5194/tc-7-303-2013.

Geweke, J., and S. Porter-Hudak (1983), The estimation and application of long memory time series models, *J. Time Ser. Anal.*, *4*(4), 221–238.

Gleckler, P. J., et al. (2012), Human-induced global ocean warming on multidecadal timescales, *Nat. Clim. Change*, *2*(7), 524–529.

Gonzalez-Rouco, J. F., H. Beltrami, E. Zorita, and H. von Storch (2006), Simulation and inversion of borehole temperature profiles in surrogate climates: Spatial distribution and surface coupling, *Geophys. Res. Lett.*, *33*, L01703, doi:10.1029/2005GL024693.
Granger, C. W. J., and M. J. Morris (1976), Time series modelling and interpretation, *J. R. Stat. Soc., Ser. A*, *139*(2), 246–257.
Grant, K. M., E. J. Rohling, M. Bar-Matthews, A. Ayalon, M. Medina-Elizalde, C. B. Ramsey, C. Satow, and A. P. Roberts (2012), Rapid coupling between ice volume and polar temperature over the past 150,000 years, *Nature*, *491*(7426), 744–747.
Gregory, J. M., J. A. Lowe, and S. F. B. Tett (2006), Simulated global-mean sea level changes over the last half-millennium, *J. Clim.*, *19*(18), 4576–4591, doi:10.1175/JCLI3881.1.
Gregory, J. M., et al. (2013), Twentieth-century global-mean sea level rise: Is the whole greater than the sum of the parts?, *J. Clim.*, *26*(13), 4476–4499, doi:10.1175/JCLI-D-12-00319.1.
Griffies, S. M., and R. J. Greatbatch (2012), Physical processes that impact the evolution of global mean sea level in ocean climate models, *Ocean Modell.*, *51*(0), 37–72.
Grinsted, A., J. Moore, and S. Jevrejeva (2010), Reconstructing sea level from paleo and projected temperatures 200 to 2100, *Clim. Dyn.*, *34*(4), 461–472, doi:10.1007/s00382-008-0507-2.
Hamlington, B. D., and P. R. Thompson (2015), Considerations for estimating the 20th century trend in global mean sea level, *Geophys. Res. Lett.*, *42*, 4102–4109, doi:10.1002/2015GL064177.
Hanna, E., et al. (2011), Greenland Ice Sheet surface mass balance 1870 to 2010 based on Twentieth Century Reanalysis, and links with global climate forcing, *J. Geophys. Res.*, *116*, D24121, doi:10.1029/2011JD016387.
Hasselmann, K. (1976), Stochastic climate models. Part I. Theory, *Tellus*, *28*(6), 473–485.
Hay, C. C., E. Morrow, R. E. Kopp, and J. X. Mitrovica (2015), Probabilistic reanalysis of twentieth-century sea-level rise, *Nature*, *517*(7535), 481–484.
Holgate, S. J. (2007), On the decadal rates of sea level change during the twentieth century, *Geophys. Res. Lett.*, *34*, L01602, doi:10.1029/2006GL028492.
Houston, J. R., and R. G. Dean (2011), Sea-level acceleration based on U.S. tide gauges and extensions of previous global-gauge analyses, *J. Coastal Res.*, *27*(3), 409–417, doi:10.2112/JCOASTRES-D-10-00157.1.
Ishii, M., and M. Kimoto (2009), Reevaluation of historical ocean heat content variations with time-varying XBT and MBT depth bias corrections, *J. Oceanogr.*, *65*(3), 287–299.
Jacob, T., J. Wahr, W. T. Pfeffer, and S. Swenson (2012), Recent contributions of glaciers and ice caps to sea level rise, *Nature*, *482*(7386), 514–518.
Jevrejeva, S., A. Grinsted, J. C. Moore, and S. Holgate (2006), Nonlinear trends and multiyear cycles in sea level records, *J. Geophys. Res.*, *111*, C09012, doi:10.1029/2005JC003229.
Jevrejeva, S., J. C. Moore, A. Grinsted, and P. L. Woodworth (2008), Recent global sea level acceleration started over 200 years ago?, *Geophys. Res. Lett.*, *35*, L08715, doi:10.1029/2008GL033611.
Jorda, G. (2014), Detection time for global and regional sea level trends and accelerations, *J. Geophys. Res. Oceans*, *119*, 7164–7174, doi:10.1002/2014JC010005.
Kemp, A. C., B. P. Horton, J. P. Donnelly, M. E. Mann, M. Vermeer, and S. Rahmstorf (2011), Climate related sea-level variations over the past two millennia, *Proc. Natl. Acad. Sci. U. S. A.*, *108*(27), 11,017–11,022.
Kopp, R. E., F. J. Simons, J. X. Mitrovica, A. C. Maloof, and M. Oppenheimer (2013), A probabilistic assessment of sea level variations within the last interglacial stage, *Geophys. J. Int.*, *193*(2), 711–716.
Kwiatkowski, D., P. C. B. Phillips, P. Schmidt, and Y. Shin (1992), Testing the null hypothesis of stationarity against the alternative of a unit root: How sure are we that economic time series have a unit root?, *J. Econometrics*, *54*(1–3), 159–178.
Lambeck, K., M. Anzidei, F. Antonioli, A. Benini, and A. Esposito (2004), Sea level in roman time in the central Mediterranean and implications for recent change, *Earth Planet. Sci. Lett.*, *224*(3–4), 563–575.
Lambeck, K., C. D. Woodroffe, F. Antonioli, M. Anzidei, W. R. Gehrels, J. Laborel, and A. J. Wright (2010), Paleoenvironmental records, geophysical modeling, and reconstruction of sea-level trends and variability on centennial and longer timescales, in *Understanding Sea-Level Rise and Variability*, pp. 61–121, Wiley-Blackwell. John Wiley and Sons Ltd., Chichester, U. K.
Large, W., and S. Yeager (2009), The global climatology of an interannually varying air–sea flux data set, *Clim. Dyn.*, *33*(2–3), 341–364.
Leclercq, P. W., J. Oerlemans, and J. G. Cogley (2011), Estimating the glacier contribution to sea-level rise for the period 1800–2005, *Surv. Geophys.*, *32*(4–5), 519–535.
Levitus, S., et al. (2012), World ocean heat content and thermosteric sea level change (0–2000 m), 1955–2010, *Geophys. Res. Lett.*, *39*, L10603, doi:10.1029/2012GL051106.
Marcos, M., and A. Amores (2014), Quantifying anthropogenic and natural contributions to thermosteric sea level rise, *Geophys. Res. Lett.*, *41*, 2502–2507, doi:10.1002/2014GL059766.
Marzeion, B., A. H. Jarosch, and M. Hofer (2012), Past and future sea-level change from the surface mass balance of glaciers, *Cryosphere*, *6*(6), 1295–1322.
Marzeion, B., J. G. Cogley, K. Richter, and D. Parkes (2014), Attribution of global glacier mass loss to anthropogenic and natural causes, *Science*, *345*(6199), 919–921.
Masters, D., R. S. Nerem, C. Choe, E. Leuliette, B. Beckley, N. White, and M. Ablain (2012), Comparison of global mean sea level time series from TOPEX/Poseidon, Jason-1, and Jason-2, *Mar. Geod.*, *35*, 20–41.
Merrifield, M. A., S. T. Merrifield, and G. T. Mitchum (2009), An anomalous recent acceleration of global sea level rise, *J. Clim.*, *22*(21), 5772–5781, doi:10.1175/2009JCLI2985.1.
Milne, G. A., W. R. Gehrels, C. W. Hughes, and M. E. Tamisiea (2009), Identifying the causes of sea-level change, *Nat. Geosci.*, *2*(7), 471–478.
Munk, W. (2002), Twentieth century sea level: An enigma, *Proc. Natl. Acad. Sci.*, *99*(10), 6550–6555.
Nicholls, R. J., and A. Cazenave (2010), Sea-level rise and its impact on coastal zones, *Science*, *328*(5985), 1517–1520.
Nicholls, R. J., P. P. Wong, V. R. Burkett, J. O. Codignotto, J. E. Hay, R. F. McLean, S. Ragoonaden, and C. D. Woodroffe (2007), Coastal systems and low-lying areas, in *Climate Change 2007: Impacts, Adaptation and Vulnerability. Contribution of Working Group II to the Fourth Assessment Report of the Intergovernmental Panel on Climate Change*, Cambridge Univ. Press, Cambridge, U. K.
Otto-Bliesner, B. L., N. Rosenbloom, E. J. Stone, N. P. McKay, D. J. Lunt, E. C. Brady, and J. T. Overpeck (2013), How warm was the last interglacial? New model-data comparisons, *Philos. Trans. R. Soc. A*, *371*(2001). [Available at http://rsta.royalsocietypublishing.org/content/371/2001/20130097.]
Palma, W. (2007), *Long-Memory Time Series: Theory and Methods*, Wiley-Interscience. John Wiley & Sons Inc., Hoboken, N. J.
Payne, A. J., A. Vieli, A. P. Shepherd, D. J. Wingham, and E. Rignot (2004), Recent dramatic thinning of largest West Antarctic ice stream triggered by oceans, *Geophys. Res. Lett.*, *31*, L23401, doi:10.1029/2004GL021284.

Percival, D. B., and A. T. Walden (1993), *Spectral Analysis for Physical Applications: Multitaper and Conventional Univariate Techniques*, Cambridge Univ. Press, Cambridge, U. K.
Percival, D. B., J. E. Overland, and H. O. Mofjeld (2001), Interpretation of north pacific variability as a short- and long-memory process, *J. Clim.*, *14*(24), 4545–4559.
Phillips, P. C. B., and P. Perron (1988), Testing for a unit root in time series regression, *Biometrika*, *75*(2), 335–346, doi:10.2307/2336182.
Pierce, D. W. (2001), Distinguishing coupled ocean–atmosphere interactions from background noise in the north pacific, *Prog. Oceanogr.*, *49*(1–4), 331–352, doi:10.1016/S0079-6611(01)00029-5.
Pritchard, H. D., S. R. M. Ligtenberg, H. A. Fricker, D. G. Vaughan, M. R. van den Broeke, and L. Padman (2012), Antarctic ice-sheet loss driven by basal melting of ice shelves, *Nature*, *484*(7395), 502–505.
Ray, R. D., and B. C. Douglas (2011), Experiments in reconstructing twentieth-century sea levels, *Prog. Oceanogr.*, *91*(4), 496–515.
Rignot, E., J. E. Box, E. Burgess, and E. Hanna (2008), Mass balance of the Greenland ice sheet from 1958 to 2007, *Geophys. Res. Lett.*, *35*, L20502, doi:10.1029/2008GL035417.
Rignot, E., S. Jacobs, J. Mouginot, and B. Scheuchl (2013), Ice-shelf melting around Antarctica, *Science*, *341*(6143), 266–270, doi:10.1126/science.1235798.
Roe, G. H. (2011), What do glaciers tell us about climate variability and climate change?, *J. Glaciol.*, *57*(203), 567–578, doi:10.3189/002214311796905640.
Roe, G. H., and M. A. O'Neal (2009), The response of glaciers to intrinsic climate variability: Observations and models of late-Holocene variations in the Pacific Northwest, *J. Glaciol.*, *55*, 839–854, doi:10.3189/002214309790152438.
Rohling, E. J., K. Grant, C. Hemleben, M. Siddall, B. A. A. Hoogakker, M. Bolshaw, and M. Kucera (2008), High rates of sea-level rise during the last interglacial period, *Nat. Geosci*, *1*(1), 38–42.
Russell, G. L., V. Gornitz, and J. R. Miller (2000), Regional sea level changes projected by the NASA/GISS atmosphere-ocean model, *Clim. Dyn.*, *16*(10–11), 789–797, doi:10.1007/s003820000090.
Schaefer, J. M., et al. (2009), High-frequency Holocene glacier fluctuations in New Zealand differ from the northern signature, *Science*, *324*(5927), 622–625.
Schmith, T., S. Johansen, and P. Thejll (2012), Statistical analysis of global surface temperature and sea level using cointegration methods, *J. Clim.*, *25*(22), 7822–7833, doi:10.1175/JCLI-D-11-00598.1.
Slangen, A. B. A., J. A. Church, X. Zhang, and D. Monselesan (2014), Detection and attribution of global mean thermosteric sea level change, *Geophys. Res. Lett.*, *41*, 5951–5959, doi:10.1002/2014GL061356.
Solow, A. R. (1990), Discriminating between models: An application to relative sea level at Brest, *J. Clim.*, *3*(7), 792–796.
Steig, E. J., et al. (2013), Recent climate and ice-sheet changes in West Antarctica compared with the past 2,000 years, *Nat. Geosci.*, *6*(5), 372–375.
Stocker, T., D. Qin, G.-K. Plattner, M. Tignor, S. Allen, J. Boschung, A. Nauels, Y. Xia, V. Bex, and P. Midgley (Eds.) (2013), *Climate Change 2013: The Physical Science Basis. Contribution of Working Group I to the Fifth Assessment Report of the IPCC*, Cambridge Univ. Press., Cambridge University Press, N. Y.
Storch, H., E. Zorita, and J. González-Rouco (2008), Relationship between global mean sea-level and global mean temperature in a climate simulation of the past millennium, *Ocean Dyn.*, *58*(3), 227–236, doi:10.1007/s10236-008-0142-9.
Storch, H. V., and F. W. Zwiers (1999), *Statistical Analysis in Climate Research*, Cambridge Univ. Press, Cambridge, U. K.
Tai, C.-K., and C. Wagner (2011), Sampling errors of the global mean sea level derived from TOPEX/Poseidon altimetry, *Acta Oceanol. Sinica*, *30*(6), 12–18.
Trenberth, K. E., J. T. Fasullo, and M. A. Balmaseda (2014), Earth's energy imbalance, *J. Clim.*, *27*(9), 3129–3144, doi:10.1175/JCLI-D-13-00294.1.
Vermeer, M., and S. Rahmstorf (2009), Global sea level linked to global temperature, *Proc. Natl. Acad. Sci. U. S. A.*, *106*(51), 21,527–21,532.
Visser, H., S. Dangendorf, and A. C. Petersen (2015), A review of trend models applied to sea level data with reference to the ''acceleration-deceleration debate'', *J. Geophys. Res. Oceans*, *120*, 3873–3895, doi:10.1002/2015JC010716.
Wenzel, M., and J. Schröter (2010), Reconstruction of regional mean sea level anomalies from tide gauges using neural networks, *J. Geophys. Res.*, *115*, C08013, doi:10.1029/2009JC005630.
Wingham, D. J., A. Shepherd, A. Muir, and G. J. Marshall (2006), Mass balance of the Antarctic ice sheet, *Philos. Trans. R. Soc. A*, *364*(1844), 1627–1635.
Wu, Z., N. E. Huang, S. R. Long, and C.-K. Peng (2007), On the trend, detrending, and variability of nonlinear and nonstationary time series, *Proc. Natl. Acad. Sci.*, *104*(38), 14,889–14,894.
Wunsch, C. (1999), The interpretation of short climate records, with comments on the North Atlantic and southern oscillations, *Bull. Am. Meteorol. Soc.*, *80*(2), 245–255.
Wunsch, C. (2016), Global ocean integrals and means, with trend implications, *Annu. Rev. Mar. Sci.*, *8*(1), 1–33, doi:10.1146/annurev-marine-122414-034040.
Wunsch, C., and P. Heimbach (2013a), Dynamically and kinematically consistent global ocean circulation and ice state estimates, in *Ocean Circulation and Climate: A 21st Century Perspective*, 2nd ed., edited by G. Siedler et al., Academic Press, Elsevier, Oxford, U. K.
Wunsch, C., and P. Heimbach (2013b), Two decades of the Atlantic Meridional Overturning Circulation: Anatomy, variations, extremes, prediction, and overcoming its limitations, *J. Clim.*, *26*(18), 7167–7186, doi:10.1175/JCLI-D-12-00478.1.
Wunsch, C., R. M. Ponte, and P. Heimbach (2007), Decadal trends in sea level patterns: 1993–2004, *J. Clim.*, *20*(24), 5889–5911.